1-1-2017

Deterministic and Random Isogeometric Analysis of Fluid Flow in Unsaturated Soils

Shahriar Shahrokhabadi

Deterministic and random Isogeometric analysis of fluid flow in unsaturated soils

By

Shahriar Shahrokhabadi

A Thesis
Submitted to the Faculty of
Mississippi State University
in Partial Fulfillment of the Requirements
for the Degree of Master of Science
in Civil Engineering
in the Department of Civil and Environmental Engineering

Mississippi State, Mississippi

December 2017

Deterministic and random Isogeometric analysis of fluid flow in unsaturated soils

By

Shahriar Shahrokhabadi

Approved:

_____

Farshid Vahedifard
(Major Professor)

_____

John F. Peters
(Committee Member)

_____

Shantia Yarahmadian
(Committee Member)

_____

James L. Martin
(Graduate Coordinator)

_____

Jason M. Keith
Dean
Bagley College of Engineering

Name: Shahriar Shahrokhabadi

Date of Degree: December 1, 2017

Institution: Mississippi State University

Major Field: Civil Engineering

Major Professor: Dr. Farshid Vahedifard

Title of Study: Deterministic and random Isogeometric analysis of fluid flow in unsaturated soils

Pages in Study 92

Candidate for Degree of Master of Science

The main objective of this research is to use IGA as an efficient and robust alternative for numerical simulation of unsaturated seepage problems. Moreover, this research develops an IGA-based probabilistic framework that can properly account for the variability of soil hydraulic properties in the simulations. In the first part, IGA is used in a deterministic framework to solve a head-based form of Richards' equation. It is shown that IGA is able to properly simulate changes in pore pressure at the soils interface. In the second part of this research, a new probabilistic framework, named random IGA (RIGA), is developed. A joint lognormal distribution function is used with IGA to perform Monte Carlo simulations. The results depict the statistical outputs relating to seepage quantities and pore water pressure. It is shown that pore water pressure, flow rate, etc. change considerably with respect to standard deviation and correlation of the model parameters.

DEDICATION

To my beloved ***Shirin***.

ACKNOWLEDGEMENTS

I would like to express my deepest gratitude to my advisor, Dr. Farshid Vahedifard. Throughout these years, Dr. Vahedifard was not just a teacher, but he also was my intimate friend. I appreciate his support, patience, and encouragement.

I would like to also send a great thanks to Dr. Manav Bhatia, for his infinite supply of comments and suggestions, kindness, and patience throughout the past years.

I would like to express my appreciation to my graduate committee members: Dr. Peters for his theoretical insight and friendship and Dr. Yahrahmadian for his kindness and support.

I would also like to extend a huge thanks to my colleagues. Each of whom have provided me with the best group of friends and classmates.

Last but not certainly the least, I would like to send out massive thanks to my parents whom I have not had a chance to meet for four years.

TABLE OF CONTENTS

LIST OF TABLES

LIST OF FIGURES

CHAPTER I

INTRODUCTION

1.1 Background

Fluid flow and heat transport in porous media are of interest in many fields of engineering and science. In particular, researchers in geomechanics or geotechnical engineering are interested in subsurface modeling where it includes flow or heat transport in geological media. Fluid components including liquids, gases, and gas-liquid phases fill the non-solid spaces (i.e., fractures, cavities, pore voids) in porous media. Water is the most important fluid among different types of fluids in environmental and hydrological context. Subsurface water often includes soil moisture of unsaturated zone and groundwater of saturated zone. The saturated zone forms strata above impervious layers and below the groundwater free surface, where the voids are fully filled with water. The unsaturated zone (vadose zone) is a moist layer between the groundwater surface and the ground surface, where only a fraction of the voids is occupied by water and the other part is filled by gaseous phase (usually air). Unsaturated flow represents two fluid phases (water and air). However, it is common to consider the gas phase constant at the atmospheric level, which simplifies the unsaturated flow problem to a one-phase model. One-phase variably saturated porous media is the subject of study in many fields of

engineering such as petroleum, geotechnical engineering, and material research for industrial porous media. In particular, the study of infiltration processes for the monitoring the water front movement from ground surface to the water table is the interesting topic in soil science and subsurface hydrology (Diersch, 2013).

Incorporating unsaturated soil mechanics into geotechnical engineering practice requires solving the governing equation that represents the variations in moisture, hydraulic conductivity, degree of saturation, etc. due to infiltration/evaporation. Richards (1930) presented a second order partial differential equation (PDE) that shows the one-phase flow mechanism in variably saturated soils. There are numerous analytical and numerical solutions to solve the governing equation (e.g., Ashcroft et al., 1962; Warrick et al., 1991; Shahraiyni and Ashtiani, 2009; Guerrero et al., 2010; Namin, et al., 2012). However, analytical solutions are limited to simple geometries and boundary conditions (Philip, 1957; Parlange, 1971; Broadbridge et al., 1988; Parlange et al., 1999) whereas numerical methods are more applicable for general unsaturated problems. Thus, there is a growing demand for improvement in the accuracy and performance of numerical methods (e.g., Huyakorn, et al., 1986; Celia et al., 1990; Gottardi and Venutelli, 1992; Wu, 2010).

This research attempts to address some of the aforementioned needs and gaps by introducing Isogeometric analysis (IGA) for solving unsaturated seepage problems in deterministic and probabilistic manners.

1.2 Objectives

The main objective of this research is to introduce and investigate the performance of IGA as an efficient and robust alternative for numerical simulation of

single-phase unsaturated seepage problems. In addition, it is intended to develop an IGA-based probabilistic framework that can properly account for the variability of soil hydraulic properties in modeling unsaturated seepage problems.

1.3 Scope and Contributions

In the presented thesis, the second chapter introduces an IGA procedure to obtain a head-based solution to the Richards equation for unsaturated flow in porous media. IGA uses Non-Uniform Rational B-Spline (NURBS) as the shape functions, which provide a higher level of inter-element continuity in comparison with Lagrange shape functions. The semi-discrete nonlinear algebraic equations are solved using a combination of implicit backward-Euler time-integration and Newton-Raphson scheme. The time-step size is adaptively controlled based on the rate of change of the pore pressure. The results from the proposed formulation are compared and verified against an analytical solution for one-dimensional transient unsaturated flow in a homogenous soil column. The proposed method is then applied to four more complex problems including two-dimensional unsaturated flow in a two-layered soil and a semi-circular furrow. The performance of IGA against the conventional finite element method for solving transient seepage problems is comprehensively evaluated and disused.

In the third chapter, a new probabilistic framework, named Random IGA (RIGA), is developed by combining IGA and random fields to numerically simulate unsaturated soil problems. The proposed framework benefits from computationally efficient IGA solutions, and properly accounts for the variability of unsaturated soil parameters by utilizing random field theory. Two constitutive models commonly used to describe the behavior of unsaturated soils, the Soil Water Retention Curve (SWRC) and Hydraulic

Conductivity Function (HCF), are considered under the proposed RIGA method. A database of unsaturated hydraulic properties is used to investigate the variability of SWRC and HCF model parameters for different soils. Random field concepts with statistical homogeneity (fixed mean, standard deviation, and spatial correlation) are implemented to generate SWRC and HCF model properties considering a joint lognormal distribution function among the model parameters. The joint lognormal distribution function is used with IGA to perform Monte Carlo simulations. The number of realizations in the Monte Carlo simulation accounts for the effect of stochastic soil parameters in unsaturated soil analysis. The application of the proposed RIGA is then illustrated by simulating unsaturated seepage in two example problems, including a one-dimensional flow in a rectangular domain and a two-dimensional infiltration problem in a semi-circular furrow.

CHAPTER II

HEAD-BASED ISOGEOMETRIC ANALYSIS OF TRANSIENT FLOW IN UNSATURATED SOILS

This chapter has been published as a journal article in Computers and Geotechnics, Volume 84: pp. 183-197, doi: 10.1016/j.compgeo.2016.11.018). The original paper may be accessed at: http://dx.doi.org/ 10.1016/j.compgeo.2016.11.018. Furthermore, the paper has been reformatted and replicated herein with minor modifications in order to outfit the purposes of this thesis.

2.1 Introduction

Transient flow in variably saturated porous media is a common interest in many research studies. Its application covers a high range of disciplines from soil science and subsurface hydrology to material research for industrial porous media, geotechnical and petroleum engineering (Diersch, 2013). In geotechnical engineering, fluid flow in unsaturated soils has shown to play a controlling role in various practical problems including slope stability (Griffiths and Lu, 2005; Lu and Godt, 2013; Robinson et al., 2016; Vahedifard et al., 2016a), lateral earth pressure (Vo et al., 2016), reinforced soil structures (Vahedifard, et al., 2016b), and bearing capacity of foundations (Oh and Vanapalli, 2012; Vahedifard, et al., 2015). Loss of suction and the subsequent reduction in soil's effective stress, due to steady or transient flow can adversely impact the

performance and integrity of variably saturated slopes and earthen structures (Richards, 1931; Robinson and Vahedifard, 2016).

From physical point of view, the air pressure can be assumed constant and fluid transportation is simply governed by Richards' equation which is the combination of generalized Darcy's law and mass continuity equation (Richards, 1931; Krabbenhøft, 2007). Richards' equation is considerably nonlinear because of highly variable effective conductivity that varies from very dry to fully saturated conditions. This variation results in a nonlinear relation between negative pore pressure and degree of saturation. The nonlinear nature of transient flow in unsaturated medium restricts the analytical solutions to few problems with simple boundary conditions (Philip, 1957; Parlange, 1971; Broadbidge and White, 1988; Parlange et al., 1999; Guerrero and Skaggs, 2010; Jaiswal et al., 2011). For general unsaturated problems, numerical methods are more applicable than analytical methods. Numerical methods that represent Richards' equation can be classified into three general forms of continuous equations: moisture-based, head-based, and mixed form.

Moisture-based (θ-based) formulation represents the governing equation in terms of moisture content. The moisture form generally performs very well when implemented in an iterative procedure and allows the use of large time steps. However, this form is only applicable to strictly unsaturated and homogenous conditions (Diersch, 2013). Head-based (h-based) form formulates the governing equation based on pressure head. This form is applicable to both saturated and unsaturated conditions and it can be used to model heterogeneous media as well. Nevertheless, its performance encounters difficulties, especially for problems involving infiltration into very dry soils. Very short

time steps are usually implemented to prevent divergence in the iterative solutions (Diersch, 2013). In an attempt to take advantages of both moisture- and head-based frameworks, the primary variable switching technique has been proposed (Forsyth et al., 1995; Diersch and Perrochet, 1999). This technique uses the moisture content as the primary variable when the domain is partially saturated and the pressure head as the primary variable when the domain is fully saturated. Despite the simplicity of the concept, there is still the possibility of divergence during the iterative procedure. For instance, in the Finite Element Method (FEM), the solution procedure may diverge if a given node with a degree of saturation below the switching criteria changes to fully saturated conditions during subsequent iterations. This problem is intensified as the mesh is refined and the wetting front covers a greater number of nodes in the associated time step (Krabbenhøft, 2007). Moreover, with respect to any form of governing equation, the efficiency and robustness of the results are highly influenced by spatial and temporal discretization methods as well as the linearization methods for nonlinear equations. For spatial discretization, the finite difference method (shahraiyni and Ashtiani, 2009; Ashcroft et al. 1962; Celia et al. 1990), FEM (Gottardi and Venutelli, 1992; Prasad, 2001; Wu, 2010), and the finite volume method (Arampatzis, 2000) are commonly used numerical methods while the finite deference is usually reserved for time discretization. For solving nonlinear equations, Picard and Newton-Raphson methods are popular schemes, which are vastly used in transient flow simulations in porous medium (Diersch, 2013).

While conventional numerical methods are successful in the simulation of transient flow problems in variably saturated soils, it is still desirable to develop more

efficient analysis methods. In recent years, Isogeometric analysis (IGA) has been increasingly employed in variety of engineering fields like plates (Valizadeh et al., 2013), incompressibility (Bazilevs et al., 2006), poroelasticity with fully saturated conditions (Irzal et al., 2013), flow regime in shale (Shahrokhabadi et al., 2014), among others. As discussed in the previous studies, IGA offers advantageous features including exactness of reproducing the geometry, higher-order continuity, and simpler mesh generation and mesh refinement procedures in comparison to alternative numerical methods. Extending IGA applications to different fields and examining advantages and disadvantages of using different types of splines in IGA have been increasingly investigated in recent years.

Nguyen et al. (2014) utilized IGA in unsaturated flow problems in the moisture-based form and introduced a successful framework including NURBS basis for spatial discretization and the implicit backward-Euler method for time discretization. However, the proposed solution is limited to homogenous problems and their solution is unable to simulate mixed unsaturated-saturated conditions. Moreover, they used constant time steps in the time integration scheme which is not computationally cost effective.

In the present study, we propose a head-based method implementing IGA to solve transient flow in heterogeneous unsaturated soils. This numerical approach utilizes NURBS basis functions for spatial discretization which benefits from the high-order continuity of IGA interpolation. The implicit backward-Euler method with adaptive time-stepping is used for time marching. This technique utilizes larger time step sizes where the rate of changes in the pore pressure is not significant, while decreasing the time step size when the changes in pore pressure are considerable and affect the solution convergence. In order to avoid oscillation at the wetting front, the lumped mass matrix

technique is used for numerical integration (Diersch, 2013) and the Newton-Raphson method is employed to solve the nonlinear equations.

The rest of chapter 2 is organized as follow: Section 2.2 describes the methodology of the presented study, in which the governing equation, variational statement, IGA spatial discretization, and time discretization are explained. In Section 2.3, the proposed method is benchmarked against a one dimensional (1D) analytical solution representing homogenous soil (Srivastava and Yeh, 1991). The application of the proposed IGA method is further extended in Section 2.4 which presents the implementation of higher order IGA in a highly nonlinear problem (referred to as Celia et al.'s (1990) problem) and comparison with an alternative FEM solution. Then numerical solution is implemented to a semi-circular furrow under high rate of infiltration. The accuracy and applicability of the method for heterogeneous medium is investigated through two numerical examples. The first example shows a 1D two-layer soil system (referred to as Brunone et al.'s (2003) problem) and results are compared with results from quadratic Lagrangian FEM. The second example represents a two dimensional (2D), two-layered soil subjected to infiltration.

2.2 Methodology

2.2.1 Governing equations

Since Richards' equation is only one flow equation, it requires the choice of primary and secondary variables. In the *h*-based formulation, the head is introduced as the primary variable and the multidimensional generalization of the governing equation is expressed as:

$$\left(\frac{\theta}{\phi}S_o + C(\psi)\right)\frac{\partial h}{\partial t} = \nabla.[k_r(\psi)K\nabla h] \tag{2.1}$$

where θ is the moisture content, ϕ is the porosity, S_o is the specific storage coefficient, h is the total head, ψ is the pressure head, $k_r(\psi)$ is relative conductivity function, K is the tensor of saturated hydraulic conductivity, ∇ is the gradient operator, and $C(\psi)$ is the moisture capacity function. In this work, a general form of K is considered enabling simulation of isotropic/anisotropic and homogenous/heterogeneous soils.

After obtaining the primary variable (h) from Eq. (2.1), ψ can be easily calculated based on classical soil mechanics concepts. Subsequently, a parameterized retention curve (e.g., Gardner (1958), or van Genuchten (1980) and Mualem (1976)) can be used to introduce θ, k_r, and C functions:

$$\textit{Gardner: } \theta(\psi) = \theta_r + (\theta_s - \theta_r)e^{-\alpha_G\psi} \tag{2.2a}$$

$$\textit{VGM: } \theta(\psi) = \begin{cases} \theta_r + (\theta_s - \theta_r)(1 + |\alpha_V\psi|^n)^{-m} & \psi < 0 \\ \theta_s & \psi \geq 0 \end{cases} \tag{2.2b}$$

Effective degree of saturation (S_e) is defined based Eq. (2.2a) or (2.2b) as:

$$S_e = \frac{\theta(\psi) - \theta_r}{\theta_s - \theta_r} \tag{2.3}$$

Subsequently the relative hydraulic conductivity is defined:

$$\textit{Gardner: } k_r(\psi) = e^{-\alpha_G\psi} \tag{2.4a}$$

$$\textit{VGM: } k_r(S_e) = S_e^{1/2}[\,1 - \left(1 - S_e^{\frac{1}{m}}\right)^m\,]^2 \tag{2.4b}$$

where θ_r and θ_s are residual and saturated moisture contents, respectively, α_G is Gardner's curve fitting coefficient, α_V and n are VGM's fitting parameters, and m can be assumed as $m = 1 - \frac{1}{n}$.

Finally, the moisture capacity function can be obtained by introducing the first derivative of Eq. (2.2):

$$\textit{Gardner: } C(\psi) = \frac{\partial \theta}{\partial \psi} = -\alpha(\theta_s - \theta_r)e^{-\alpha_G \psi} \tag{2.5a}$$

$$\textit{VGM: } C(\psi) = \frac{\partial \theta}{\partial \psi} = \frac{mn\alpha_V |\alpha_V \psi|^{n-1}}{(1+|\alpha_V \psi|^n)^{m+1}}(\theta_s - \theta_r) \tag{2.5b}$$

The h-based form of Richards' equation can produce considerable mass balance errors. This drawback is caused by the addition of $C(\psi)$ in the approximation of the storage term (left hand side of Eq. (2.1)). Obtaining $C(\psi)$ based on the chord slope approximation method has been introduced as a solution to preserve mass conservation (Diersch, 2013). In this study, the chord slope approximation is used instead of direct analytical derivatives to avoid any mass balance error. Appendix A presents the necessary expressions for approximating C using the chord slope approximation.

2.2.2 Isogeometric Analysis for Head-Based solution

Let Ω be the spatial domain, $\Omega \in \mathrm{R}^{\mathrm{D}}$, where D denotes the spatial dimensionality. Let Γ specify the boundary of Ω which is $\Gamma_D \cup \Gamma_N$, where Γ_D and Γ_N represent the boundaries with Dirichlet and Neumann conditions, respectively. The Galerkin variational statement for Eq. (2.1) states that h can be found such that for any arbitrary function U ($U = 0$ on Γ_D):

$$\int_\Omega \left\{ \left(\frac{\theta}{\phi} S_o + C(\psi) \right) \frac{\partial h}{\partial t} - \nabla . [k_r(\psi) K \nabla h] \right\} . U d\Omega = 0 \tag{2.6}$$

Following standard discretization notations, the continuous head is approximated by:

$$h(\boldsymbol{x}, t) \approx R(\boldsymbol{x})\hat{h}(t) \tag{2.7}$$

where $R(\boldsymbol{x})$ shows the shape functions and $\boldsymbol{x}$ represents the coordinate of spatial nodes. Using integration by parts, the resulting nonlinear matrix system is:

$$\boldsymbol{O}(\psi).\dot{\widehat{\boldsymbol{h}}} + \boldsymbol{K}(\psi).\widehat{\boldsymbol{h}} - \boldsymbol{F} = \boldsymbol{0} \tag{2.8}$$

$$\boldsymbol{O} = \sum_e \delta_{ij} \int_{\Omega^e} \left(\frac{\theta}{\phi} S_o + C(\psi)\right)^e R_{ij}\, d\,\Omega^e \tag{2.9}$$

$$\boldsymbol{K} = \sum_e \int_{\Omega^e} \nabla R^T.\left(k_r{}^e(\psi) K^e.\nabla R\right) d\,\Omega^e \tag{2.10}$$

$$\boldsymbol{F} = \sum_e \int_{\Gamma^e} \mathrm{Rq}^e d\,\Gamma^e \tag{2.11}$$

where $\boldsymbol{O}$ is the lumped-mass matrix, $\dot{\widehat{\boldsymbol{h}}}$ represents the changes in the h vector with respect to time, $\boldsymbol{K}$ is the permeability matrix, $\boldsymbol{F}$ is the force vector, q^e represents infiltration or evaporation rates from elements boundary, and δ_{ij} is Kronecker-delta property. The mass-lumping technique presented in Eq. (2.9) is only applicable for IGA and linear FEM. For higher order FEM, the mass-lumping technique discussed in Appendix B should be considered. In addition to Eqs. (2.9) and (2.10), the interpolation of the moisture capacity and relative conductivity over the element e is introduced as:

$$C^e(\psi) = \sum_j R^e{}_j\, C^e(\psi^e{}_j) \tag{2.12}$$

$$k_r{}^e(\psi) = \sum_j R^e{}_j\, k_r{}^e(\psi^e{}_j) \tag{2.13}$$

where the pressure head ψ at local node j of element e is evaluated from the solution h ($\psi^e{}_j = h^e{}_j - y_j$, in which y_j shows the elevation of node j).

The shape functions in Eq. (2.7) are formed by NURBS basis functions. The linear combination of NURBS basis functions with a given set of control points is used to shape a curve of order p (Hughes, 2005):

$$\widehat{\boldsymbol{C}}(\xi) = \sum_i^n R_{i,p}(\xi)\boldsymbol{P}_i \tag{2.14}$$

where n is the number of control points, $\boldsymbol{P}_i$ is the i^{th} control point coordinate, and $R_{i,p}(\xi)$ is the NURBS basis function defined by:

$$R_{i,p}(\xi) = \frac{N_{i,p}(\xi)w_i}{\sum_{j=1}^{n} N_{j,p}(\xi)w_j} \tag{2.15}$$

where $N_{i,p}(\xi)$ and w_i are the i^{th} B-spline basis function of order p and the assigned weight to i^{th} control point, respectively. $N_{i,p}(\xi)$ is constructed based on a knot vector $\boldsymbol{\Theta}(\xi)$ in the parametric space which is in an ascending sequence of real numbers. It is common to define the parametric space $\boldsymbol{\Theta}(\xi)$ as:

$$\boldsymbol{\Theta}(\xi) = \{\xi_1, \xi_2, \dots, \xi_i, \dots, \xi_{n+p+1}\} \qquad \xi \in [0,1] \tag{2.16}$$

where ξ_i shows the i^{th} knot.

Open knot vectors have the Kronecker-delta property at the boundaries and the direct imposition of essential boundary conditions is applicable when they are used for spatial discretization. Open knot vectors are formed if the first and last knot (ξ_1, ξ_{n+p+1}) are repeated $p+1$ times, implying curves include discontinuities (c^{-1} continuity). Moreover, the basis functions can be interpolatory at intermediate knots where they are repeated p times. This implies that curves include corresponding control points in the physical space with c^0 continuity (Hughes et al. 2005). This property allows introducing soil layers with definite interfaces. The B-spline basis functions are defined based on the recursive Cox-de Boor algorithm (De Boor, 1972):

$$N_{i,0}(\xi) = \begin{cases} 1 & \xi_i \le \xi < \xi_{i+1} \\ 0 & otherwise \end{cases} \quad \text{for } p = 0 \tag{2.17a}$$

$$N_{i,p}(\xi) = \frac{\xi - \xi_i}{\xi_{i+p} - \xi_i} N_{i,p-1}(\xi) + \frac{\xi_{i+p+1} - \xi}{\xi_{i+p+1} - \xi_{i+1}} N_{i+1,p-1}(\xi) \quad \text{for } p \ge 1 \tag{2.18}$$

Figure 2.1 shows a set of quadratic B-spline basis functions which are used in one of the example problems solved in Section 2.4. This sort of knot vector interpolates the first and last knots ($\xi = 0,1$) in the knot vector which results in interpolation of the corresponding nodes in the physical geometry. This is also true for the intermediate knot ($\xi = 0.5$). This property allows exact definition of external and internal boundaries. The internal boundaries are defined as the intersection of two regions with different hydraulic properties.

Formation and insertion of knot and control points are the key steps to shape geometry and h-refinement in IGA. Here, the formation of geometry is discussed first and it is followed by knot insertion description which can be performed by inserting a single knot once or multiple times.

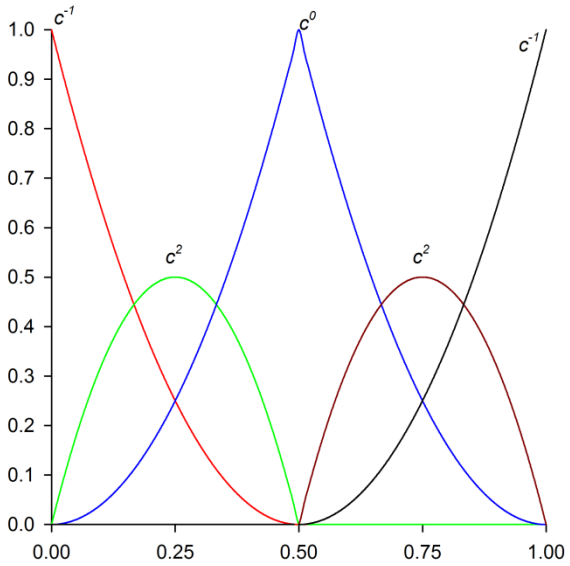

Figure 2.1 Quadratic basis functions for the open knot vector $\boldsymbol{\Theta}(\xi) = \{0, 0,0,0.5,0.5,1,1,1\}$.

Consider a set of points $\{Q_k\}$ $(k = 1, 2, \dots, n)$ on the geometry of the problem. In order to interpolate these points with NURBS basis functions of order *p*, we need to assign a parameter $\bar{\xi}$ to each Q_k, and select an appropriate knot vector $(\xi) = \{\xi_1, \xi_2, \dots, \xi i, \dots, \xi n+p+1\}$ $\xi \in [0,1]$. We can form up to $(n) * (n)$ system of linear equations using:

$$Q_k = \widehat{\boldsymbol{C}}(\bar{\xi}) = \sum_i^n R_{i,p}(\bar{\xi})\boldsymbol{P}_i \tag{2.19}$$

where $\boldsymbol{P}_i$ represents *n* unknown control points. The next step is to determine $\bar{\xi}$ and (ξ). There are three common methods to find $\bar{\xi}$: equally spaced, chord length, and centripetal method (Piegl, 1966). In this study, the chord length method is used. In this method, d is introduced as the total chord length

$$d = \sum_{k=1}^{n-1} |Q_{k+1} - Q_k| \tag{2.19}$$

Then the following statement is defined by assuming $\bar{\xi}_1 = 0$:

$$\bar{\xi}_k = \bar{\xi}_{k-1} + \frac{|Q_k - Q_{k-1}|}{d} \quad k = 2,3, \dots, n \tag{2.20}$$

Subsequently, the corresponding knots, which are able to reflect the distribution of $\bar{\xi}_k$, are defined based on the averaging technique:

$$\Theta(\xi) = \begin{cases} \xi_1 = \cdots = \xi_p = 0 \\ \xi_{j+p-1} = \frac{1}{p}\sum_{i=j}^{j+p-1} \bar{\xi}_i \quad j = 2,3, \dots, n-p \\ \xi_{n+1} = \cdots = \xi_{n+p+1} = 1 \end{cases} \tag{2.21}$$

Furthermore, using Eq. (2.21) along with Eq. (2.20) in Eq. (2.18) leads to a system of linear equations from which $\boldsymbol{P}$ can be obtained easily. Further information regarding geometry formation using NURBS can be found in "The NURBS Book" (Piegl, 1966).

Refinement in IGA can be done by knot insertion without changing the geometry of the problem. Introducing the extended knot vector $\widetilde{\boldsymbol{\Theta}}(\xi) = \{\xi_1 = \tilde{\xi}_1, \tilde{\xi}_2 \dots \tilde{\xi}_{n+m+p+1} = \xi_{n+p+1}\}$ leads to defining new $n+m$ basis functions. Subsequently, the corresponding new $n+m$ control points $\widetilde{\boldsymbol{P}}$ are formed by a linear combination of the original control points:

$$\widetilde{\boldsymbol{P}} = \boldsymbol{T}^{\boldsymbol{p}}\boldsymbol{P} \tag{2.22}$$

where

$$T_{ij}^{q} = \begin{cases} 1 & \tilde{\xi}_i \in [\,\xi_j,\, \xi_{j+1}) \\ 0 & otherwise \end{cases} \tag{2.23}$$

$$T_{ij}^{q+1} = \frac{\tilde{\xi}_{i+q} - \xi_j}{\xi_{j+q} - \xi_j} T_{ij}^{q} + \frac{\xi_{j+q+1} - \tilde{\xi}_{i+q}}{\xi_{j+q+1} - \xi_{j+1}} T_{ij+1}^{q} \quad \text{for } q = 0,1,\dots,p-1 \tag{2.24}$$

Further information for p and h refinement can be found in Hughes et al. (2005).

Eq. (2.14) can be easily extended to higher spatial dimensions (2D and 3D) using the tensor product concept. Subsequently, a NURBS surface, $S(\xi,\eta)$ of order p and q with respect to ξ and η-direction, can be formed as:

$$S(\xi,\eta) = \sum_i^n \sum_j^m R_{i,j}^{p,q}(\xi,\eta)\boldsymbol{P}_{i,j} \tag{2.25}$$

In Eq. (2.25), $\boldsymbol{P}_{i,j}$ represents the coordinates of control points in 2D while $R_{i,j}^{p,q}(\xi,\eta)$ shows the bivariate NURBS basis functions in parametric coordinates of ξ and η. The formation of bivariate basis function follows:

$$R_{i,j}^{p,q}(\xi,\eta) = \frac{N_{i,p}(\xi)M_{j,q}(\eta)w_{i,j}}{\sum_{k=1}^{n}\sum_{l=1}^{m} N_{k,p}(\xi)M_{l,q}(\eta)w_{k,l}} \tag{2.26}$$

where w shows the 2D weights and $M_{j,q}(\eta)$ is the basis function of order q for j^{th} knot in the η-direction. The shape functions in IGA, as used in the current study, have the following advantageous properties (Hughes, 2005):

- NURBS basis functions satisfy partition of unity: $\sum_{i=1}^{n} R_{i,p} = 1$.

- The shape functions are always positive; this property is useful for mass-lumping techniques (Nguyen et al., 2014).
- The basis functions of order p are $p - m_i$ times differentiable (c^{p-m_i}), m_i shows the multiplicity of the i^{th} knot.
- The support of $R_{i,p}$ is compact and covers $[\xi_i,\xi_{i+p+1}]$. Thus, the number of nodes per element is $(p+1)$ and $(p+1)\times(q+1)$ for 1D and 2D problems, respectively.

2.2.3 Temporal Discretization

The nonlinear matrix system (Eq. (2.8)) is solved in time with suitable initial conditions (IC). The fully-implicit time-marching scheme is used in backward-Euler (BE) framework. The formulation of BE with an automatic error-controlled time step helps to speed up the h-based solution in comparison with the fixed time step scheme (Diersch, 2013). Expanding Eq. (2.8) based on the BE time discretization introduces the discrete residual of the h-based Richards' equation as:

$$R_{t+1}(\widehat{\boldsymbol{h}}) = \left(\frac{\boldsymbol{O}(\psi_{t+1})}{\Delta T_t} + \boldsymbol{K}(\psi_{t+1})\right).\widehat{\boldsymbol{h}}_{t+1} - \left(\frac{\boldsymbol{O}(\psi_{t+1})}{\Delta T_t}\right).\widehat{\boldsymbol{h}}_t - \boldsymbol{F} \qquad (2.27)$$

Since the mass matrix ($\boldsymbol{O}$) and the permeability matrix ($\boldsymbol{K}$) are dependent on the solution itself, iterative methods are needed to solve Eq. (2.27) for $\widehat{\boldsymbol{h}}_{t+1}$. Utilizing the Newton-Raphson iteration method leads to the final form of Richards' equation for IGA:

$$\left(\frac{\boldsymbol{O}(\psi_{t+1}^{\kappa})}{\Delta T_t} + \boldsymbol{K}(\psi_{t+1}^{\kappa})\right).\Delta\widehat{\boldsymbol{h}}_{t+1}^{\kappa+1} = \left(\frac{\boldsymbol{O}(\psi_{t+1}^{\kappa})}{\Delta T_t}\right).\widehat{\boldsymbol{h}}_t - \boldsymbol{J}(\psi_{t+1}^{\kappa}).\widehat{\boldsymbol{h}}_{t+1}^{\kappa} + \boldsymbol{F} \qquad (2.28)$$

where t counts the time steps, κ denotes the iteration numbers, $\Delta\widehat{\boldsymbol{h}}_{t+1}^{\kappa+1}$ is the increment for $\kappa+1$ iteration ($\widehat{\boldsymbol{h}}_{t+1}^{\kappa+1} = \widehat{\boldsymbol{h}}_{t+1}^{\kappa} + \Delta\widehat{\boldsymbol{h}}_{t+1}^{\kappa+1}$), and $\boldsymbol{J}(\psi_{t+1}^{\kappa})$ shows the partial Jacobian matrix as:

$$\boldsymbol{J}(\psi_{t+1}^{\kappa}) = \left(\frac{\boldsymbol{o}(\psi_{t+1}^{\kappa})}{\Delta T_t} + \boldsymbol{K}(\psi_{t+1}^{\kappa})\right) \tag{2.29}$$

2.2.3.1 Adaptive Time Steps

Selecting the appropriate time step significantly affects the solution performance. Large time steps during the initial solution phase can lead to inaccurate results or even divergence of the solution. On the other hand, small time steps lead to considerable computational costs when the solution is stable and close to steady state conditions. The adaptive time steps method, originally developed by Gresho (1978), controls the solution process with a local time prediction. In this approach, the time step size is automatically updated with respect to requirements of temporal accuracy. The adaptive time step procedure is robust and computationally inexpensive in that the time step size increases whenever possible or decreases if necessary. Several studies have demonstrated the advantages of adaptive time stepping for solving the Richards equation (Miller, 2006). The scheme is based on Local Truncation Error (LTE) estimation:

$$\boldsymbol{d}_{t+1} = \widehat{\boldsymbol{h}}_{t+1} - \widehat{\boldsymbol{h}}_{t} \tag{2.30}$$

where d_{t+1} is the residual between the approximate solution in the next time step ($\widehat{\boldsymbol{h}}_{t+1}$) and the exact solution in the current time step ($\widehat{\boldsymbol{h}}_{t}$). It is assumed that the exact solution is introduced at the beginning of each time step. Subsequently, if the current LTE is kept for the next time step, the potential step size can be obtained as:

$$\Delta T_{t+1} = \Delta T_t \left(\frac{\varepsilon}{\|\boldsymbol{d}_{t+1}\|}\right)^{1/2} \tag{2.31}$$

In Eq. (2.31), ε is the prescribed error tolerance and $\|\boldsymbol{d}_{t+1}\|$ is Root Mean Square (RMS) norm for $\boldsymbol{d}_{t+1}$. The fitness of the predicted time step from Eq. (2.31) should be evaluated for the next time step. This procedure is conducted by checking three following conditions:

- *Condition 1. If* $\Delta T_{t+1} \geq \Delta T_t$

The increase in time step is allowed and the predicted ΔT_{t+1} is acceptable for the next time step. However, it has been shown that it is practically beneficial to limit the upper bound of the next time step to:

$$\Delta T_{t+1}^{prac} = min(\Delta T_{t+1}, \Delta T_{max}, \beta \Delta T_t) \tag{2.32}$$

where ΔT_{t+1}^{prac} is the applicable time step size that is used for the next time step, ΔT_{max} is the maximum user-defined time step size, and β the rate of change in the time step size ($\beta = \frac{\Delta T_{t+1}}{\Delta T_t}$) which can be 1,2,3,….

- *Condition* 2. If $\gamma \Delta T_t \leq \Delta T_{t+1} \leq \Delta T_t$

Where γ is typically 0.85, the solution $\widehat{\boldsymbol{h}}_{t+1}$ is acceptable but the predicted time step size should not be changed ($\Delta T_{t+1} = \Delta T_t$).

- *Condition 3. If* $\Delta T_{t+1} \leq \gamma \Delta T_t$

The solution $\widehat{\boldsymbol{h}}_{t+1}$ is not acceptable and there is no update for the next time step. This condition enforces the algorithm to repeat the current time step with a reduced time step size as:

$$\Delta T_t^{red} = \frac{{\Delta T_t}^2}{\Delta T_{t+1}} \left(\frac{\varepsilon}{\|\boldsymbol{d}_{t+1}\|}\right) \tag{2.33}$$

where ΔT_t^{red} shows the reduced time step size. The new solution again will be evaluated against error conditions and further step reduction is allowed if the third condition (Eq. (2.33)) governs the solution. However, the solution algorithm must restart the overall time stepping with new error condition (ε) or the initial time step (ΔT_0), if the number of reduction cycles reaches twelve cycles.

2.2.4 Head-Based Solution Algorithm

The main steps of the proposed h-based solution, utilizing IGA and adaptive time step, for solving Richards' equation are summarized in Box 2.1.

Box 2.1. Algorithm for h-based solution using IGA and adaptive time steps.
1. Discretize the problem geometry with NURBS mesh.
2. Define problem properties, i.e., $K, S_o, \theta_r, \theta_s, \Delta T_0$, ...
3. Define B.C (Γ_D ,Γ_N) and allocate related node IDs in the mesh.
4. Loop over time steps: $t = 0,1,\ldots$ Or $\|\boldsymbol{d}_{t+1}\| < \varepsilon_{steady}$
   4.1 Loop over *Iterations*: $\kappa = 0,1,\ldots$Or until convergence $\|\Delta\widehat{\boldsymbol{h}}\| < \varepsilon_{conver}$
      4.1.1 Update the Residual vector and Jacobian matrix based on Eq. (2.28, 2.29)
      4.1.2 Update the increment: $\Delta\widehat{\boldsymbol{h}} = (\boldsymbol{J}_{t+1}^{\kappa})^{-1} R_{t+1}^{\kappa}$
      4.1.3 Update $\widehat{\boldsymbol{h}}_{t+1}^{\kappa+1} = \widehat{\boldsymbol{h}}_{t+1}^{\kappa} + \Delta\widehat{\boldsymbol{h}}$
   END for iterations
   4.2 Update $\|\boldsymbol{d}_{t+1}\|$
   4.3 Update ΔT_{t+1} based on Eq. (2.31)
   4.4 IF $\Delta T_{t+1} \geq \Delta T_t$ then update $\widehat{\boldsymbol{h}}_{t+1}$ and ΔT_{t+1} using Eq. (2.32)
      Else IF $\gamma \Delta T_t \leq \Delta T_{t+1} \leq \Delta T_t$ then update $\widehat{\boldsymbol{h}}_{t+1}$ and $\Delta T_{t+1} = \Delta T$
      Else **Do** not update $\widehat{\boldsymbol{h}}_{t+1}$ **,** reduce time step using Eq. (2.33), and repeat current time step.
   4.5 Post processing and visualization in selected time steps.
      END for time steps

In the above algorithm, ε_{steady} and ε_{conver} are the prescribed tolerances for the steady state condition and convergence criteria.

2.3 Validation

In this section, the proposed IGA formulation is validated against an analytical solution and also compared with conventional FEM analysis for a benchmark problem. Srivastava and Yeh (1991) proposed an analytical solution for one-dimensional (vertical) transient unsaturated flow problem subjected to infiltration/evaporation in a homogenous soil column. They used Gardner's equations (Eq. (2.2a) and Eq. (2.4a)) to introduce hydraulic conductivity, pressure and retention curve. To evaluate the accuracy and performance of the proposed solution based on IGA, a 3 m column of soil under a prescribed infiltration (flux) is considered (Figure 2.2(a)). The datum is assumed at the bottom where the groundwater table is located. The top boundary is subjected to the infiltration rate of $q = 0.2\ md^{-1}$ while the bottom boundary is enforced to the essential boundary condition of zero ($h = 0$) and the negative ICs are distributed hydrostatically in the problem.

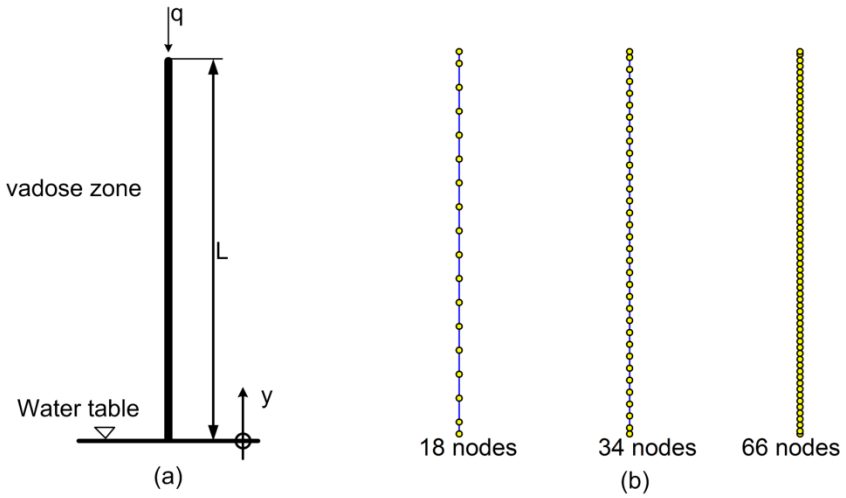

Figure 2.2 1D infiltration problem in vadose zone: a) Sketch of the unsaturated solution domain. b) Discretized domain in IGA with different node numbers.

The analytical solution of Eq. (2.1) for transient flow (i.e., negative pore pressure) for the given retention curve and hydraulic conductivity function is presented as:

$$h = \frac{\ln(\rho)}{\alpha} \tag{2.34}$$

where

$$\rho = \frac{q}{K} - \left(\frac{q}{K} - 1\right) e^{-y^*} - \frac{4q}{K} e^{\left(\frac{L^* - y^*}{2}\right)} . e^{-\frac{t^*}{2}} . \sum_{i=1}^{\infty} \frac{\sin(\lambda_i y^*) \sin(\lambda_i L^*) e^{-\lambda_i^2 t^*}}{1 + \left(\frac{L^*}{2}\right) + 2\lambda_i^2 L^*} \tag{2.35}$$

$$t^* = \frac{\alpha K t}{(\theta_s - \theta_r)}$$

$$y^* = \alpha y$$

$$L^* = \alpha L$$

In the above equations, L is the soil column length and λ_i is the i^{th} root of the characteristic equation. The characteristic equation is defined as:

$$tan(\lambda . L^*) + 2\lambda = 0 \tag{2.36}$$

For the IGA simulation, linear, quadratic, and cubic NURBS basis functions are used with the associated knot vectors:

$\boldsymbol{\Theta}(\xi) = \{\, 0,0,1,1\},\ \boldsymbol{\Theta}(\xi) = \{0, 0,0,1,1,1\},$ and $\boldsymbol{\Theta}(\xi) = \{0,0, 0,0,1,1,1,1\}$ and the corresponding control points $\boldsymbol{P} = \{0,3\},\ \boldsymbol{P} = \{0,1.5,3\},$ and $\boldsymbol{P} = \{0,1,2,3\}$, respectively. The introduced $\boldsymbol{\Theta}$ and $\boldsymbol{P}$ generate few degrees of freedom (DOFs) which are not adequate for numerical solutions. In order to generate reasonable models, the number of nodes (i.e., DOFs) is increased using non-uniform h-refinement and results are compared with the analytical solution. One of the interesting features of NURBS mesh is the automatic generation of finer mesh near boundaries. This property is very important for extremely

dry soils subjected to high rate of infiltration. The hydraulic conductivity of the boundary elements in these problems is very small and unable to transmit the water away from the boundary nodes. As a remedy, generating finer mesh near boundaries and providing a proper feedback in the matrix to the flux are key steps to alleviate this problem (Wu, 2010). Figure 2.2(b) shows the discretized geometry for 18, 34, 66 DOFs.

For comparison purposes, the benchmark problem is also solved using linear and quadratic FEM. Since linear IGA configuration can be adapted to linear FEM, the same discretized configuration (non-uniform mesh) is utilized for both FEM and IGA. However, non-uniform mesh is used for quadratic/higher-order IGA while uniform mesh is used for quadratic FEM.

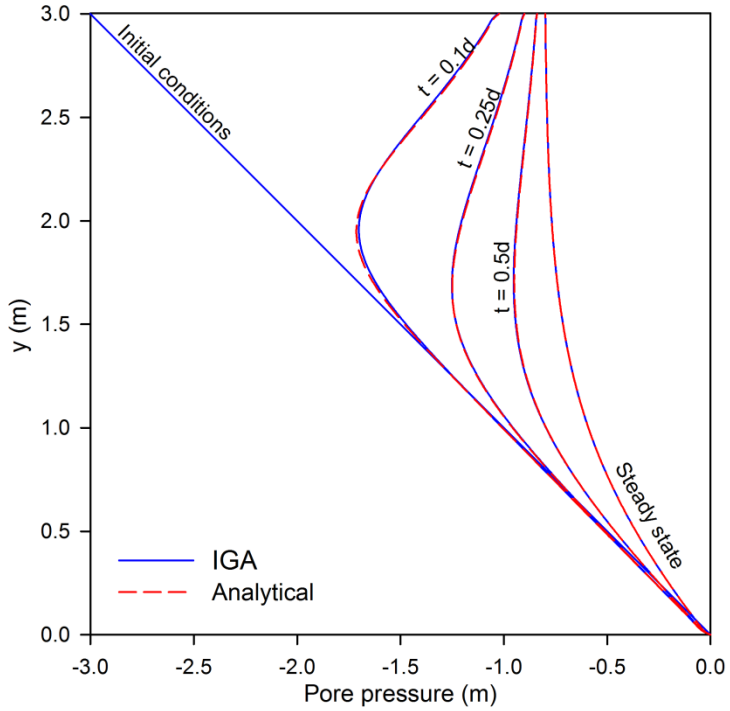

Figure 2.3 Analytical [40] and IGA solution for 1D homogenous soil under infiltration of $0.2md^{-1}$.

In order to avoid convergence issues and obtain an acceptable accuracy, the initial time steps (ΔT_0) in the adaptive time steps are chosen sufficiently small in all cases. To show more details, Table 2.1 summarizes the material properties and assumptions that are used for solving this problem. Figure 2.3 shows the pore pressure profile using the analytical solution and the proposed IGA solution (with 66 DOFs) for time intervals of t = 0.1, 0.25, 0.5 day, and steady state condition.

Table 2.1 Parameters and conditions used for homogenous soil column.

Quantity	Symbol	Value	Unit
Column length	L	3	m
Saturated conductivity	K	1.0	md^{-1}
Porosity	ϕ	0.4	
Specific Storage Coefficient	S_o	0	m^{-1}
Saturated moisture content	θ_s	0.4	1
Residual moisture content	θ_r	0.092	1
Gardner parametric model			
Fitting coefficient	α_G	2	m^{-1}
IC and BC's			
Initial conditions (IC)	h_0	0.0	m
Neumann-type BC at top	q	0.2	md^{-1}
Dirichlet-type BC at bottom	h_D	0.0	m
Method: IGA, FEM			
Initial time step size	Δt_0	0.45	s
Convergence error tolerance	ε_{conver}	10^{-4}	1
Steady state error tolerance	ε_{steady}	10^{-4}	1

Constant time steps ($\Delta T = 9\ min$) require a large computational expense with 548 time steps to capture the steady state conditions. On the other hand, 118 time steps are only needed to reach the steady state solution with the adaptive time stepping. The

range of time step sizes varies from 0.45(s) at the first time steps to 0.5 day for the last time steps and in all intervals a very good agreement is observed between the analytical and the IGA results.

For a thorough error analysis, l_2 error norm is calculated using:

$$l_2 = \left(\int_{\Omega^e} (h_{num} - h_{Anl})^2 d\Omega^e\right)^{\frac{1}{2}} \tag{2.37}$$

where h_{num} is the solution vector from numerical methods (i.e., IGA or FEM) and h_{Anl} is the solution vector from the analytical solution.

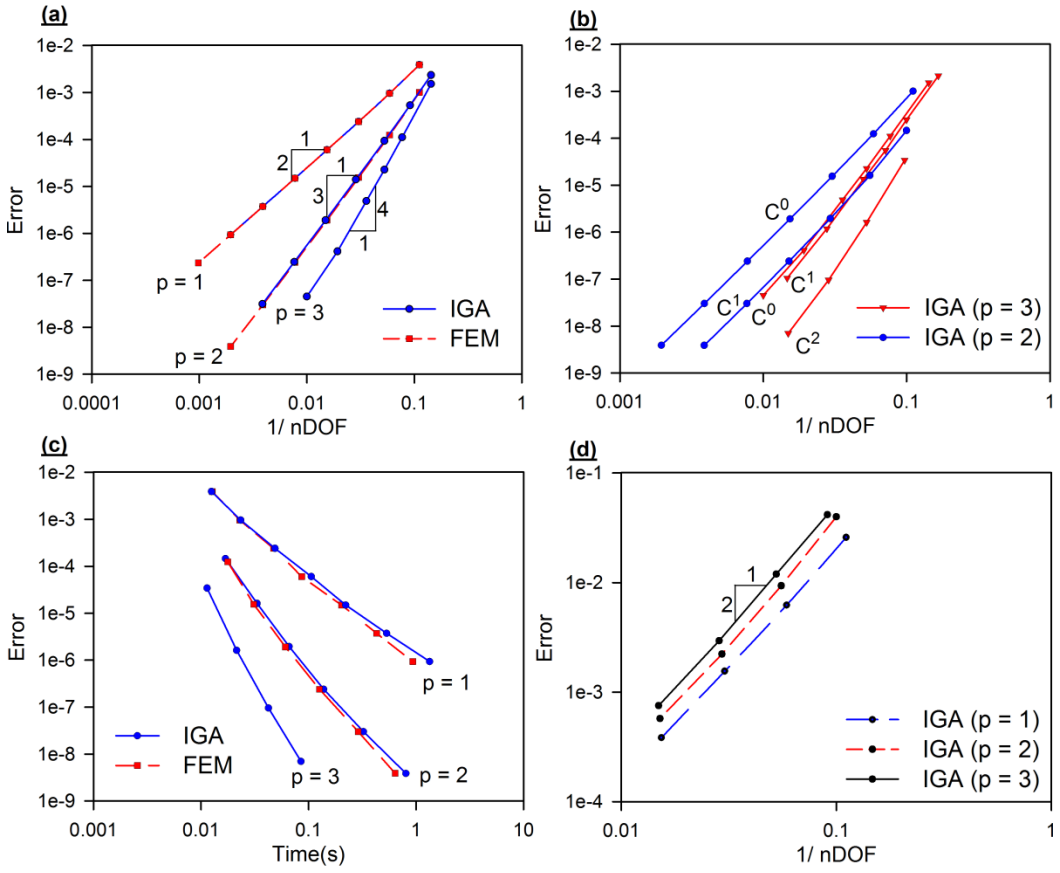

Figure 2.4 $l2$ error analysis for IGA and FEM: (a) p-refinement (steady analysis), (b) effect of inter-element discontinuity, C^m (m = 0, 1, and 2), (c) Computational time, (d) p-refinement (transient analysis).

Figure 2.4 represents the results for steady state and transient conditions using different DOFs, orders of approximation, and element continuities. Figure 2.4(a) shows the effect of p refinement while C^0 elements are used in the steady state condition. The results for linear FEM and IGA (IGA1, FEM1) are identical when a similar mesh configuration is used. Although we use a uniform mesh for quadratic FEM, the descending trend for quadratic IGA and FEM (IGA2, FEM2) is also similar. For $p = 3$, only cubic IGA (IGA3) is studied and the descending trend depicts the highest rate of convergence in comparison with the linear and quadratic IGA/FEM. In general, the results show identical trends for both IGA and FEM with the rate of convergence of $p+1$. That is, for example, the rate of convergence for $p = 2$ is equal to 3V:1H.

Figure 2.4(b) illustrates the effects of C^m (m = 0, 1, and 2) continuity on the error analysis. Considering quadratic IGA, the rate of convergence is identical for both C^0 and C^1 continuities. However, C^1 elements yield a smaller error for a given number of DOFs. The continuity analysis for cubic IGA ($p = 3$) suggests an identical rate of convergence for m = 0, 1, and 2. However, for a given number of DOFs, the error magnitude decreases by increasing the level of continuity (m). The results of error analysis demonstrate that C^2 elements have better performance in comparison with C^0 and C^1 continuities.

Figure 2.4(c) depicts the reduction in error magnitude with respect to increase in CPU time for both IGA and FEM. Generally, as expected, the computation cost grows by increasing the number of DOFs. Further, the results suggest that p-refinement leads to a decrease in both computational cost and error magnitude. It is noticeable that the computational cost for IGA and FEM algorithms are almost similar. Although FEM

shows slightly better performance in the case of higher number of DOFs, the overall difference between IGA and FEM results is negligible.

Figure 2.4(d) shows the error analysis results for IGA (p =1, 2, and 3) at t = 0.1d to examine the performance of the model under transient condition. The trend of error analysis results is found very sensitive to time discretization. For all cases which were examined, increasing DOFs could decrease error magnitude up to a certain level but beyond that, no further error reduction is observed by increasing the DOF. In the current analysis, the number of time steps is increased to $1e^5$ and it is observed that, within the depicted range of DOFs, the error analysis has a descending trend with a slope of 2V:1H. On the other hand, it should be noted that the magnitude of error is considerably higher than the state-state analysis. While beyond the scope of the current study, further studies are recommended to investigate the implementation of high-order implicit/explicit time integration schemes.

2.4 Numerical Examples

2.4.1 Celia et al.'s problem

Celia et al.'s problem is a benchmark model to represent a strong infiltration front development in a homogenous soil column. Unsaturated hydraulic constitutive equations of soil are presented by the VGM model. Celia et al. (1990) used the modified Picard method in the context of mixed formulation of Richards' equation and considered a column of 1 m length subjected to Dirichlet boundary conditions at the top and bottom. They used a constant time step ($\Delta t = 60s$) to obtain the solution for the simulation time of 1 day. Table 2.2 briefly represents the parameters and conditions that are defined for Celia et al.'s problem.

Table 2.2 Parameters and conditions used for Celia et al.'s problem.

Quantity	Symbol	Value	Unit
Column length	L	1	m
Saturated conductivity	K	$9.22e^{-5}$	md^{-1}
Porosity	ϕ	0.368	
Specific Storage Coefficient	S_o	0	m^{-1}
Saturated moisture content	θ_s	0.368	1
Residual moisture content	θ_r	0.102	1
VGM parametric model			
Fitting parameter	n	2	1
Fitting coefficient	α_V	3.35	m^{-1}
IC and BC's			
Initial conditions (IC)	ψ_0	-10	m
Dirichlet -type BC at top	ψ_D^T	-0.75	m
Dirichlet-type BC at bottom	ψ_D^B	-10	m
Method: IGA, FEM			
Initial time step size	Δt_0	0.05	s
Convergence error tolerance	ε_{conver}	10^{-4}	1
Steady state error tolerance	ε_{steady}	10^{-4}	1

In the current study, we use linear and quadratic FEM and IGA to simulate the same problem and investigate the effect of p refinement in highly nonlinear problems. For IGA and linear FEM the mass-lumping technique described in Eq. (2.9) is used which is known as the row-sum technique. However, for higher order FEM the special lumping technique that is presented in Appendix B is needed.

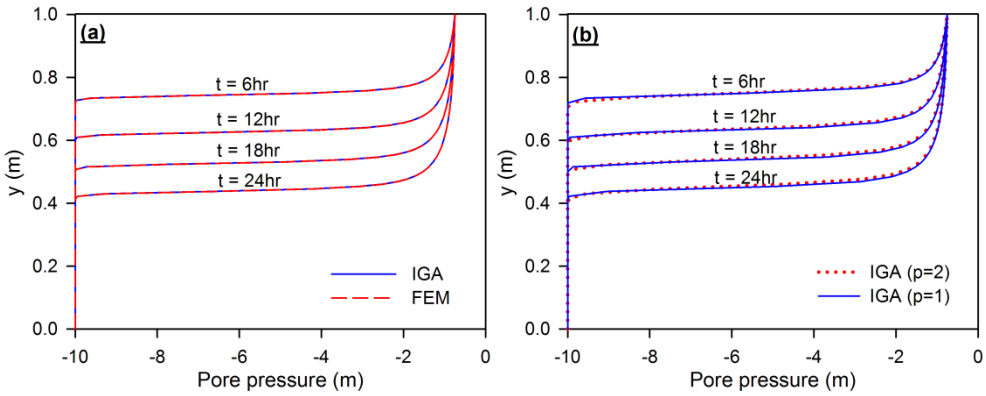

Figure 2.5 (a): Simulation of 1 day infiltration using linear IGA and FEM. (b) Comparison of linear and quadratic IGA for 1 day simulation.

Figure 2.5(a) shows the results of simulation for IGA1 and FEM1 with 65 DOFs. The time of simulation is 24 hours and the solution is presented in time intervals of 6 hours. As expected, the results are quite similar for both linear FEM and IGA. Using the mass lumping technique in Eq. (2.9) eliminates the oscillation in the solution otherwise the solution contains oscillation if consistent mass matrix is used. However, the result from higher order elements needs a detailed study. Implementing special mass lumping in the FEM2 formulation is not a successful strategy to prevent oscillation while IGA2 obtains desired results by implementing row mass lumping.

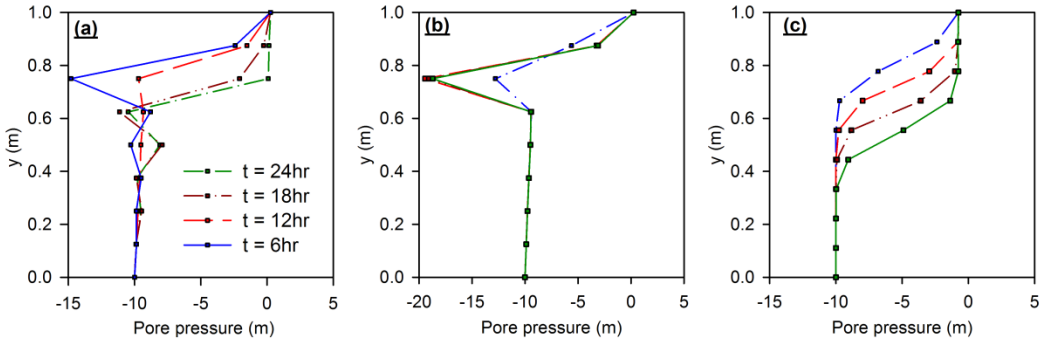

Figure 2.6 Wetting front propagation in Celia et al.'s problem (a) FEM2 with consistent mass matrix. (b) FEM2 with special mass matrix. (c) IGA2 with row mass lumping.

Figure 2.6 shows the patterns of wetting front propagation for quadratic FEM (Figures (2.6a) and (2.6b)) and IGA (Figure 2.6(c)) using 9 and 10 DOFs, respectively. The wetting front propagation versus time using FEM2 is depicted in Figure 2.6(a). The results show considerable oscillation when mass lumping is not formulated in the numerical scheme. Further, as demonstrated in Figure 2.6(b), FEM2 does not still yield proper results even using the special mass lumping technique and chord slope approximation of C (Eq. (2.5)). Following to the sharp change of pore pressure which occurs in the elements near the top boundary, C significantly increases in the corresponding nodes at the top boundary. This condition leads to the formation of a very large mass matrix while the magnitude of conductance matrix is considerably small, eventually resulting oscillatory solutions. This issue is very similar to the well-known numerical oscillation of reaction-diffusion processes when reaction dominates the physics (i.e.,Illinca and Hétu, 2008). Mass lumping is a stabilization procedure that helps alleviate these spurious oscillations. However, while this procedure is able to stabilize the FEM1 and all IGA solutions, it fails to stabilize the FEM2 solution with quadratic

Lagrange shape functions, which are C^0 continuous. This observation can be possibly attributed to the fact that the mid-node of each element in FEM2 is connected to only two nodes, while the side nodes of the element are connected to four other nodes. IGA2, on the other hand, maintains the same level of connectivity for each degree-of-freedom, thereby providing a larger support across multiple nodes in the problem domain. This, as demonstrated in Figure 2.6(c), can likely enhance the stability of the numerical discretization to simulate wetting front propagation.

Solutions of the h-based form of Richards' equation are not generally mass conservative. However, the h-based formulation can still lead to a mass-conservative solution if the moisture capacity is properly introduced in the formulation. Using chord slope approximation of moisture capacity is a remedy to this shortcoming and it has been successfully used in several h-based solutions (e.g., Wu, 1999). To examine the IGA results, mass conservation ratio is defined as the ratio of total additional mass in the domain with respect to total net flux into the domain:

$$\eta = \frac{\int_{\Omega}(\theta(t)-\theta_0)d\Omega}{\int_0^t(q_{in}-q_{out})dt} \tag{2.38}$$

where η is mass ratio, $\theta(t)$ is the moisture content at a given time, θ_0 is the initial moisture content, q_{in} and q_{out} are defined as the inward flux into system and outward flux, respectively.

The mass conversation of the h-based IGA results is examined for two cases where moisture capacity is calculated using the analytical solution (i.e., Eq. 2.5(a)) or approximated using the chord slope method. Figure 2.7 depicts the mass conservation ratios of the h-based IGA results for both cases. The analysis shows that if the analytical

solution of moisture capacity is considered in the numerical formulation, the method is not mass conservative and about 30% of mass loss occurs at the beginning of simulation. It is noticeable that an increase in p in this method leads to an increase in mass loss. However, as shown, the method using the chord slope approximation is totally mass conservative and the value of η is unity during the simulated time.

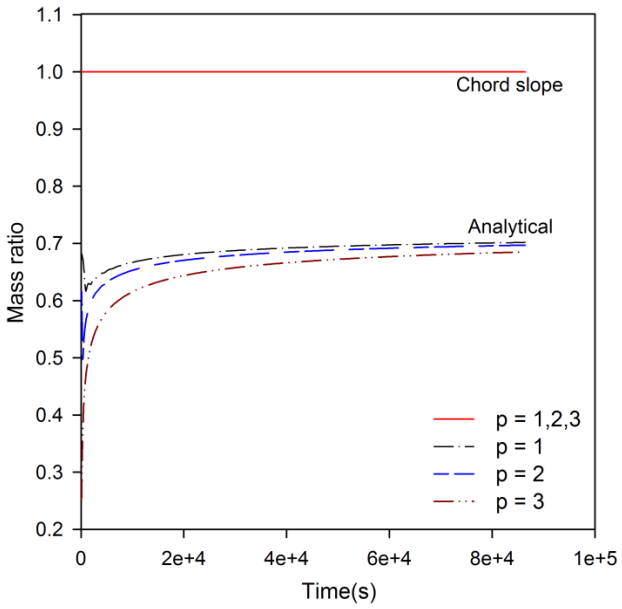

Figure 2.7 The analysis of mass conservation for Celia's problem.

2.4.2 2D Infiltration Problem in Semi-Circle Furrow

To illustrate the ability of IGA for modeling unsaturated seepage problems in complex geometries, this section presents results for IGA modeling of infiltration in a semi-circular furrow. As illustrated in Figure 2.8(a), the vadose zone is subjected to infiltration in a semi-circular region at the top while it rests on the water table at the bottom boundary. Hydrostatic distribution of pore water pressure is defined as initial

condition. The 2D problem is modeled with R = 1 m where R is the radius of furrow, and x = y = 4 m where x, y are horizontal and vertical dimensions of the model, respectively. Soil properties are taken identical to the parameters introduced in Problem 2.4.1 (Celia et al.'s problem) and the infiltration rate (q) is $8.3e^{-5}$ md^{-1}, which suggests a highly nonlinear problem due to the high rate of imposed infiltration.

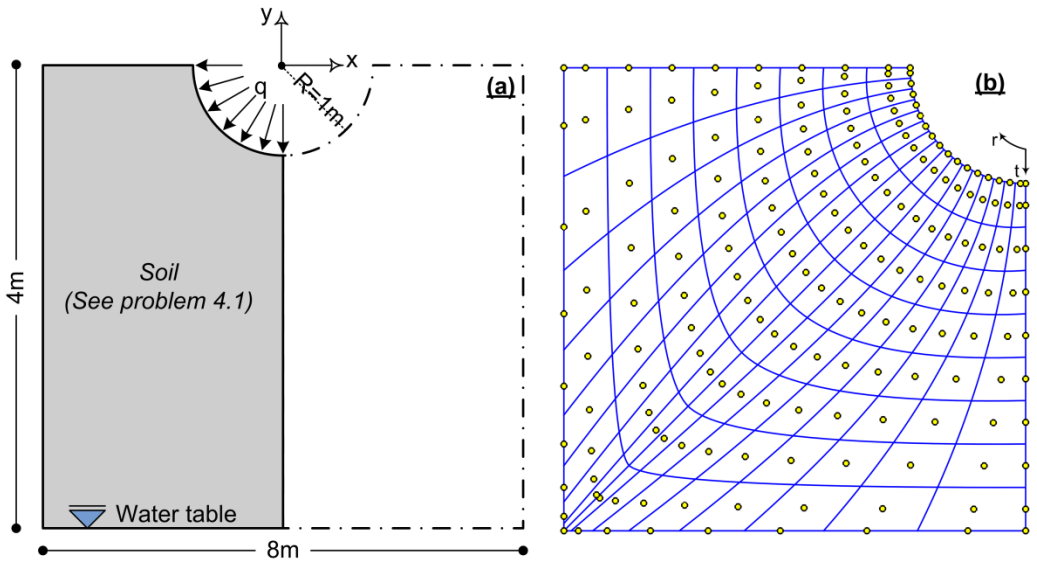

Figure 2.8 Infiltration problem in semi-circular furrow: (a) Geometry and hydraulic boundary conditions. (b) Discretized domain using quadratic IGA mesh.

Taking advantage of symmetry, only a half of the domain is considered in the simulation and the geometry is simulated via quadratic basis functions. The associated knot vectors with respect to each direction are defined as $\boldsymbol{\Theta}(\xi)_r = \{0, 0, 0, 0.5, 1, 1, 1\}$ and $\boldsymbol{\Theta}(\xi)_t = \{0, 0, 0, 1, 1, 1\}$ where r and t represent the discretization directions (see Figure 2.8(b)). The corresponding control points with respect to $\boldsymbol{\Theta}(\eta)_r$ and $\boldsymbol{\Theta}(\xi)_t$ are defined as:

$$\boldsymbol{P}_{i,j} = \begin{Bmatrix} 0 & -0.4142 & -1 & -1 & 0 & -0.75 & -2.5 & -2.5 & 0 & -3.99 & -4 & -4 \\ -1 & -1 & -0.4142 & 0 & -2.5 & -2.5 & -0.75 & 0 & -4 & -4 & -4 & 0 \end{Bmatrix} \quad (2.39)$$

To accurately simulate the semi-circle geometry at the top boundary, the following weight vector is applied to the control points:

$$w_i = \left\{1 \quad 1+\frac{1}{\sqrt{2}} \quad 1+\frac{1}{\sqrt{2}} \quad 1 \quad 1 \quad 1 \quad 1 \quad 1 \quad 1 \quad 1 \quad 1 \quad 1\right\} \quad (2.40)$$

For illustration purpose, Figure 2.8(b) shows the discretized domain with 165 DOFs while the transient simulation is performed using 612 DOFs. Figure 2.9 shows total head contours at different times of t = 0.5, 1, 3 d and steady state condition. This problem involves applying a high rate of infiltration to a dry soil. The conductivity of the nodes related to the circular boundary is small and considering the geometry of the problem, these nodes may not be able to properly transfer the moisture from the boundary nodes to the soil body. This condition can dump moisture on the elements near the boundary. However, utilizing IGA and adaptive time steps allows to successfully transmitting moisture into the soil body in this problem. Cloud of nodes near the furrow and C^1 elements associated with small time steps at the beginning stages of simulation suggest a successful remedy to alleviate large hydraulic gradients and complex geometries.

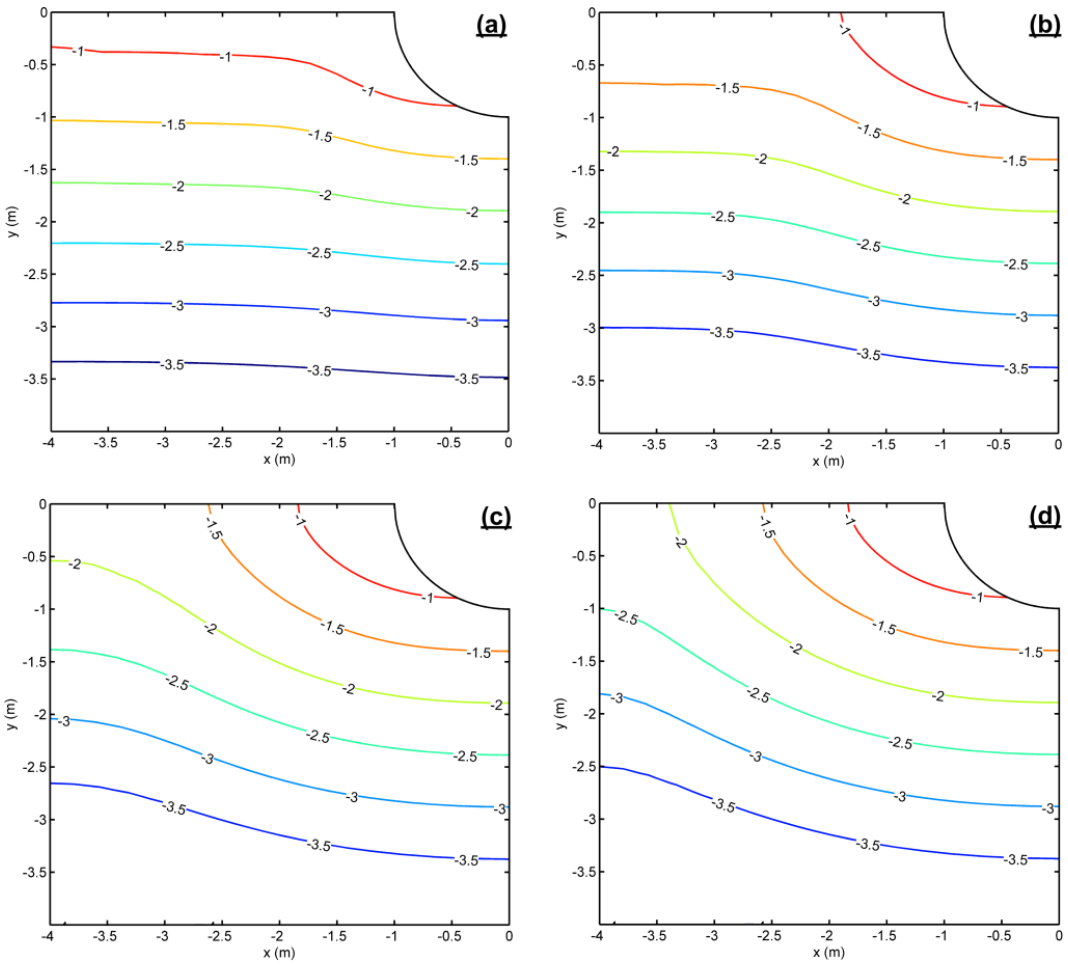

Figure 2.9 Total head contours for infiltration in semi-circular furrow at different time intervals: (a) t=0.5d (b) t =1d (c) t=3d (d) Steady state.

2.4.3 Brunone et al.'s Problem

Brunone et al. (2003) studied the transient flow problem for a heterogeneous column of soil. The flow conditions were similar to the research done by Hills et al. (1989) in which a layered soil profile made up of layers of Berino loamy fine sand at the top and Glendale clay loam at the bottom. The upper layer is exposed to an intense vertical infiltration while it has a lower hydraulic conductivity with respect to the bottom layer. Since this problem is highly nonlinear, improper IC can highly affect the accuracy

of the solution and leads to divergence. In this case, the steady state pressure head profile for the constant infiltration rate of q = 4.54 × 10^{-6} mh^{-1} is used as IC while the infiltration rate abruptly changes to q = 95 × 10^{-4} mh^{-1}. In the discretized domain, the boundary condition for the top boundary is flux (q) and the boundary condition at the bottom is a prescribed constant head. Tables 2.3 and 2.4 list further details that specify this highly nonlinear problem. As shown, Gardner's model is used to describe hydraulic constitutive equations of the soils.

Table 2.3 Parameters used for Brunone et al.'s problem.

Quantity	Symbol	Value	Unit
Column length	L	1	m
IC and BC's			
Initial conditions (IC)	h_0	Variable	m
Neumann-type BC at top	q	95e^{-4}	md^{-1}
Dirichlet-type BC at bottom	h_D	-1.0	m
IGA2			
Degree of freedom	DOF	50 and 100	1
FEM2			
Degree of freedom	DOF	50 and 100	1
Initial time step size	Δt_0	0.45	s
Convergence error tolerance	ε_{conver}	10^{-4}	1
Steady state error tolerance	ε_{steady}	10^{-4}	1

Table 2.4 Material properties used for Brunone et al.'s problem.

Layer	Thickness (m)	ϕ	θ_r	θ_s	α_G(m^{-1})	K (mh^{-1})	S_o (m^{-1})
1	0.2	0.4	0.06	0.4	10	0.01	10^{-4}
2	0.8	0.4	0.06	0.4	10	0.1	10^{-4}

To model Brunone et al.'s problem, quadratic NURBS basis functions are utilized based on knot vector $\boldsymbol{\Theta}(\xi) = \{0, 0,0,0.5,0.5,1,1,1\}$ and control points $\boldsymbol{P} = \{0,0.65,0.8,0.95,1\}$. The introduced $\boldsymbol{\Theta}$ has C^0 continuity at $\mathbf{P}_3 = 0.8$ (Figure 2.1). This property allows the introduction of a definite boundary between two soil layers. In addition, based on the aforementioned, when a boundary is interpolatory in IGA, finer elements will be automatically generated near that boundary. In order to compare the results with quadratic FEM, the same mesh configuration is used for FEM2. Two models with the number of DOFs of 50 and 100 with non-uniform mesh are analyzed and results are compared with the corresponding analytical results.

In variably saturated transient flow problems, the principal motivation behind the mass-lumping technique is the generation of a mass matrix, $\boldsymbol{O}$, which is diagonal and easily invertible. Moreover, fully implicit time marching in combination with mass lumping has shown privilege to consistent mass matrix (Diersch, 2013). In the FEM2 analysis, the special mass lumping technique is used while in IGA2 analysis the row-sum technique is used. In FEM, the row-sum technique is usually valid for linear elements where the shape functions are always positive. For higher order IGA, the lumping procedure is equivalent to the row-sum technique since IGA basis functions are always positive Hughes (2005). In conventional FEM, the higher-order shape functions could be either negative or positive, which limits the applicability of the row-sum technique.

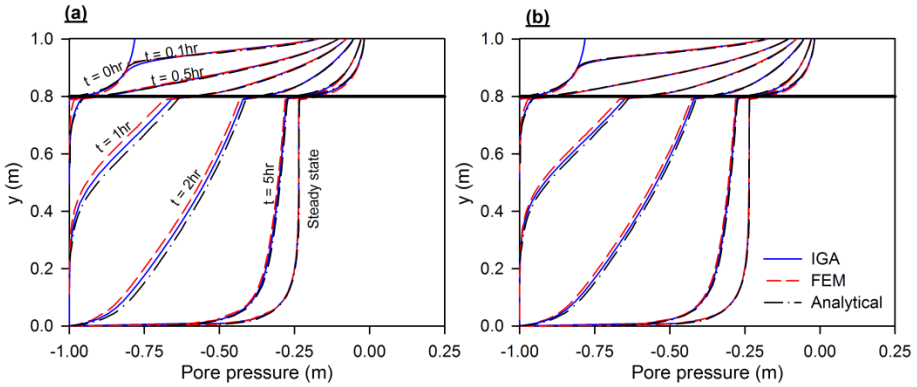

Figure 2.10 (a): Wetting front for 1D heterogeneous soil using 50 DOF for IGA2 and FEM2. (b): Wetting front for 1D heterogeneous soil using 100 DOF for IGA2 and FEM2.

The pore pressure profile for different time intervals and 50 DOFs is illustrated in Figure 2.10(a). It shows that both IGA2 and FEM2 are able to predict the wetting front properly in the top layer where the hydraulic conductivity is ten times less than the bottom layer. However, in the bottom layer, the pore pressure profile obtained by FEM2 is behind the pore pressure profile achieved by IGA2. This trend is more pronounced for time intervals of 1 and 2 hours and as time increases toward the steady state condition, the difference between IGA2, FEM2 and the analytical solution decreases. The number of DOFs is increased to 100 in Figure 2.10(b), which shows that the solutions from both IGA2 and FEM2 are closer to the analytical solution, though the predicted wetting front from FEM2 is still behind IGA2. In summary, it is seen that the results from IGA are closer to the analytical solution by increasing the DOF and *p* refinement.

2.4.4 2D Infiltration in Heterogeneous Soils

The last example shows the numerical simulation of the infiltration problem into two layers of soil in the vadose zone. This example represents a 2D geometry with 2 m

width and 3 m high subjected to a constant infiltration rate (q) at the surface for 2 days. As depicted in Figure 2.11(a), it is assumed that the infiltration is only imposed on the left part of the surface ($-1 \leq x \leq -0.5$) and the rest of the top boundary is a no-flux zone. The bottom layer lies on the water table and it enforces the essential boundary condition h = 0. While the hydraulic conductivity of the soil layer at the top is twice as the hydraulic conductivity of the bottom layer, a continuous hydrostatic distribution of pore water pressure is assumed as ICs for both layers. The internal boundary that separates two layers of soils is located at 1.5 m. Further details for material properties of soil layers and Gardner parameters are presented in Table 2.5 and 2.6, respectively.

Table 2.5 Parameters used for 2D heterogeneous problem.

Quantity	Symbol	Value	Unit
Column length	L	3	m
IC and BC's			
Initial conditions (IC)	h_0	Hydrostatic	m
Neumann-type BC at top	q	0.7	md^{-1}
Dirichlet-type BC at bottom	h_D	0.0	m
IGA (p=1,2, and 3)			
Degree of freedom	DOF	500	1
Initial time step size	Δt_0	0.45	s
Convergence error tolerance	ε_{conver}	10^{-4}	1
Steady state error tolerance	ε_{steady}	10^{-4}	1

Table 2.6 Material properties used for 2D heterogeneous problem.

Layer	Thickness(m)	ϕ	θ_r	θ_s	α_G (m^{-1})	K (mh^{-1})	S_o (m^{-1})
1	1.5	0.4	0.092	0.4	2	0.042	0
2	1.5	0.4	0.092	0.4	2	0.021	0

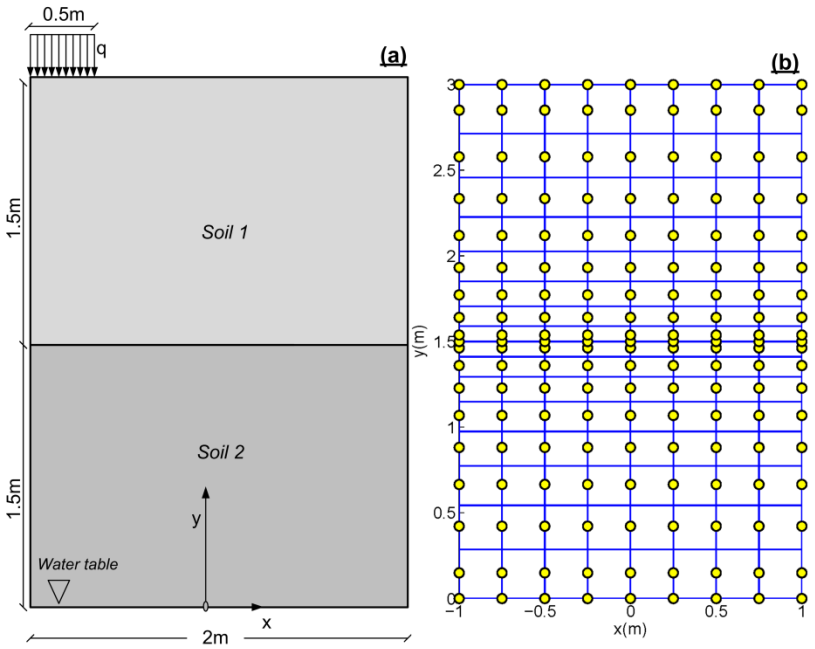

Figure 2.11 (a) Sketch of the 2D unsaturated solution domain in heterogeneous vadose zone. (b) IGA mesh based on NURBS basis function (170 DOF).

The presented problem is simulated with IGA using 500 DOFs based on NURBS basis functions and the results are compared regarding *p* refinement. Problem domain is discretized to non-monotonic element sizes since IGA mesh is finer near the boundaries. This intrinsic property of IGA is induced as a result of decrease in continuity of NURBS basis functions to c^{-1} and c^{0}. In this study, the domain boundaries (external boundaries) are generated by utilizing open knot vectors that include c^{-1} property. The generation of internal boundary is done by repeating the associate knot *p*-1 times in knot vectors which results in c^{0} continuity at the interface of two soil layers.

To discretize the problem using IGA mesh in the x and y directions, we used $\boldsymbol{\Theta}(\eta)_x = \{0,0,1,1\}$ to discretize the domain in the x direction while the order of basis function (p_x) is 1 and for the y direction, the parameters for the quadratic case (i.e.

$\boldsymbol{\Theta}(\xi)_y = \{0, 0, 0, 0.5, 0.5, 1, 1, 1\}$ with order of $p_y = 2$) are shown. The corresponding control point with respect to $\boldsymbol{\Theta}(\eta)_x$ and $\boldsymbol{\Theta}(\xi)_y$ is defined as:

$$\boldsymbol{P}_{i,j} = \begin{Bmatrix} -1 & -1 & -1 & -1 & -1 & 1 & 1 & 1 & 1 & 1 \\ 0 & 1.2 & 1.5 & 1.8 & 3 & 0 & 1.2 & 1.5 & 1.8 & 3 \end{Bmatrix} \tag{2.41}$$

The presented problem is simulated with IGA using 500 DOFs based on NURBS basis functions and the results are compared regarding *p* refinement. Problem domain is discretized to non-monotonic element sizes since IGA mesh is finer near the boundaries. This intrinsic property of IGA is induced as a result of decrease in continuity of NURBS basis functions to c^{-1} and c^{0}. In this study, the domain boundaries (external boundaries) are generated by utilizing open knot vectors that include c^{-1} property. The generation of internal boundary is done by repeating the associate knot *p*-1 times in knot vectors which results in c^{0} continuity at the interface of two soil layers.

In order to visualize the discretized domain with IGA mesh, Figure 2.11(b) represents the discretized geometry when the number of DOFs is 170. The internal boundary is located at the elevation of 1.5 m and as expected, the elements with smaller sizes are generated near the internal boundary.

The numerical simulation shows the mechanism of negative pore pressure dissipation in the selected domain for 2 days. The results of pre-selected time interval of t =0.1, 0.5, and 2 days are presented in Figure 2.12.

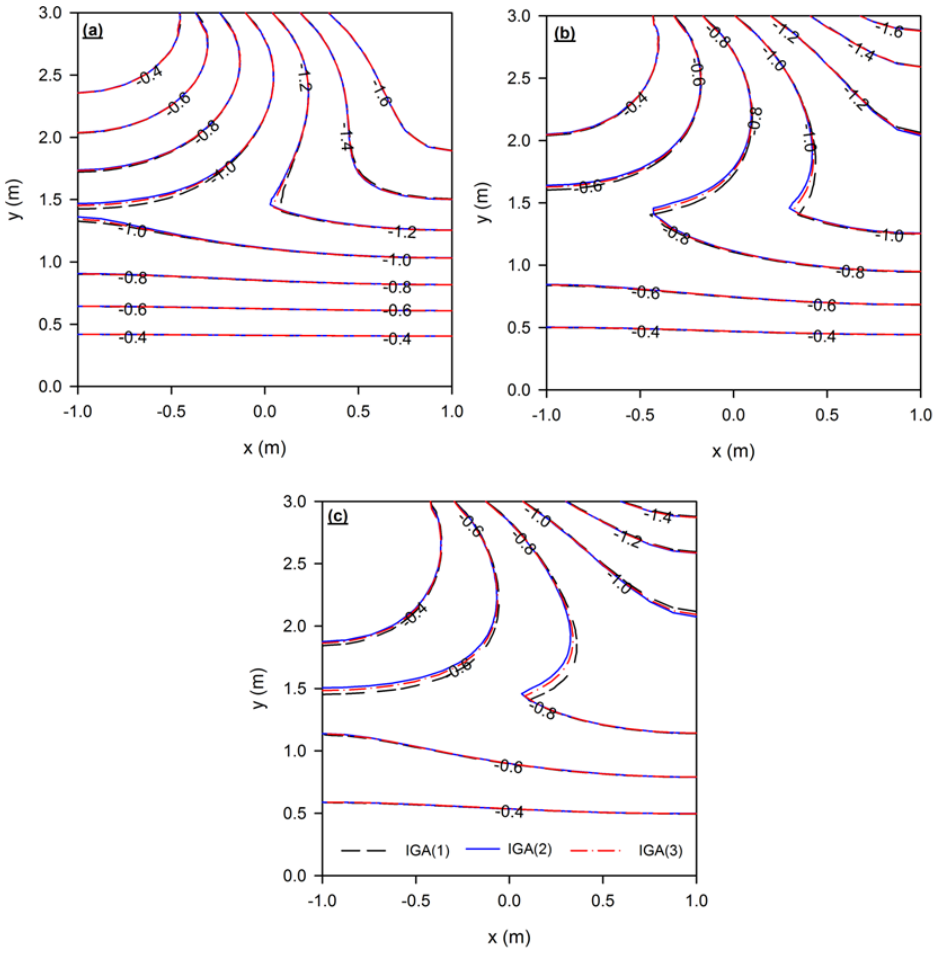

Figure 2.12 Pore pressure contours for heterogeneous soil: a) t=0.1 day, b) t=0.5 day, and c) t= 2 day.

IGA simulations (p = 1, 2, 3) represent the dissipation of negative pore pressure which occurs in a lower rate in the bottom layer. It is also noticeable that near the internal boundary, the sharp changes in pore pressure contours appear. Generally, the difference between IGA results is pronounced near this region. Sharp changes in the pore water pressure profile at the soils interface are expected. In comparison with linear approximation (IGA1), p-refinement in this study suggests that higher order approximations estimate the sharp changes closer to the internal boundary.

CHAPTER III

RANDOM ISOGEOMETRIC ANALYSIS (RIGA) FOR MODELING SEEPAGE IN UNSATURATED SOILS

This chapter has been submitted to the ASCE Journal of Engineering Mechanics as a technical paper, and it is under peer review process while this thesis has been written. This chapter has been reformatted and replicated herein with minor modifications in order to outfit the purposes of this thesis.

3.1 Introduction

The majority of natural soils are heterogeneous with highly variable properties. Soil variability can be attributed to lithological heterogeneity, uncertainty in measured data from a site, inclusion of uniform soil mass pockets with different lithology or transformation uncertainty (Phoon and Kulhawy, 1999; Elkateb et al., 2003). The first source of uncertainty shows embedded stiffer/softer layers in thicker softer/stiffer media. The second source, which is known as point variability, describes the variation in measured properties independent from the position. For instance, the permeability coefficients obtained from different samples from the same site represent point variability. Point variability in soil properties is commonly shown by Probability Density Function (PDF) (Phoon et al. 2010). The third source which attributes to the definition of spatial variability shows the variation of soil properties from one point to another in a

given medium. Spatial variability is usually defined by the spatial correlation functions (Elkateb et al., 2003; Green et al., 2015). The mathematical structure that combines point and spatial variability is termed as random field theory (Fenton and Griffiths 2008).

In conventional geotechnical engineering practice, geotechnical engineers commonly use high factors of safety and past experience to account for the effects of uncertainties in design. However, case histories show that 70% of geotechnical failures were due to poor or bad engineering judgments (Morgenstern, 2000). Therefore, the need for developing more reliable tools to consider the variability in engineering designs and analyses has been well-accepted (e.g., Fenton and Griffiths, 2003; Griffiths and Fenton, 2009, Bastani and Damircheli, 2013; Bastani and Damircheli, 2017). Random field models have successfully been employed along with the Finite Element Method (FEM) to account for the effects of variability of soil parameters (e.g., Griffiths and Fenton, 1993; Schweiger and Peschl, 2005; Zhang and Yan, 2015). In such analyses, FEM simulations account for point and spatial variability using either a stochastic approach or Monte Carlo simulation (Elkateb et al., 2003). Employing the Monte Carlo method in random field simulations needs considerably large numbers of successive simulations to accurately predict the behavior of soils with highly variable properties. Therefore, it is desirable to employ a computationally efficient solver with the Monte Carlo method for simulating the true behavior of a system. This problem is further intensified where the soil properties show a highly nonlinear behavior (e.g., unsaturated flow in porous media). It is noted the majority of the above-mentioned studies accounted for the variability of soil properties in the context of classic soil mechanics, where the soil is treated as either dry or saturated. Modeling unsaturated soil problems, as a more general case, can pose further

complexities due to a higher number of parameters needed to describe the hydro-mechanical properties of these soils and the inherent variability associated with them. Limited work (e.g., Cheng et al. 2016; Soraganvi et al. 2016; Liu et al. 2017) has been done to incorporate the effects of such variability in the simulation of unsaturated soil problems.

In this study, for the first time we combine Isogeometric analysis (IGA) and random field theory and propose a new probabilistic framework, called Random Isogeometric Analysis (RIGA), for simulating unsaturated soil problems. The proposed framework offers a computationally efficient solution, owing to IGA features, and also accounts for the variability of unsaturated soil parameters. The Soil Water Retention Curve (SWRC) and Hydraulic Conductivity Function (HCF) are considered two key constitutive equations for describing the behavior of unsaturated soils. A database of unsaturated hydraulic properties is used to investigate the variability of SWRC and HCF model parameters for different soils. Random field concepts with statistical homogeneity (fixed mean, standard deviation, and spatial correlation) are used to generate SWRC and HCF model properties. A joint lognormal distribution function is introduced to present the PDF for model parameters and it is used within IGA to perform Monte Carlo simulations of unsaturated seepage problems. Application of the proposed RIGA is then illustrated by simulating unsaturated seepage in two example problems.

3.2 Variability in hydraulic properties of unsaturated soils

3.2.1 Governing Equations

Richards' equation is commonly used to describe fluid flow in unsaturated soils. In this study, we consider a head-based formulation of Richards' equation:

$$\nabla.[k_r(s_e)K_s\nabla h] = \left(\frac{\theta}{\phi}S_0 + C(\psi)\right)\frac{\partial h}{\partial t} \quad (3.1)$$

where θ is the volumetric water content, ϕ is the porosity, S_0 is the specific storage coefficient, h is total head, ψ is matric suction, $k_r(s_e)$ is relative conductivity function, s_e is effective degree of saturation, K_s is saturated hydraulic conductivity tensor, and $C(\psi)$ is the moisture capacity. $k_r(s_e)$, K_s, ϕ, and S_0 are determined based on soil types and experimental data. Subsequently, these terms can be introduced as the sources of uncertainty in unsaturated flow analysis. In this study and for simplicity, we focused on the uncertainty imposed by the variability in $k_r(s_e)$ and K_s.

3.2.2 Point variability

Volumetric water content (θ) and matric suction (ψ) are the key parameters in defining the hydraulic properties of unsaturated soils. The θ- ψ relationship, referred to as the SWRC, can be represented by several models in the literature (e.g., Brooks and Corey, 1964; van Genuchten 1980; Fredlund and Xing, 1994). The majority of these models are developed to relate the Hydraulic Conductivity Functions (HCF) of the soils to the suction regime. For instance, van-Genuchten (1980) and Mualem (1976) (VGM) expresses hydraulic conductivity as follows:

$$\theta(\psi) = \begin{cases} \theta_r + (\theta_s - \theta_r)(1 + |\alpha_V\psi|^n)^{-m} & \psi < 0 \\ \theta_s & \psi \geq 0 \end{cases} \quad (3.2)$$

where θ_r and θ_s are residual and saturated moisture contents, respectively, α_V and n are VGM's fitting parameters representing the inverse of the air-entry head and the breadth of the soil's pore size, respectively. It is commonly assumed to $m = 1 - \frac{1}{n}$.

Based on Eq. (3.2), effective degree of saturation (s_e) is defined as:

$$s_e = \frac{\theta(\psi)-\theta_r}{\theta_s-\theta_r} \tag{3.3}$$

Subsequently, the hydraulic conductivity in unsaturated soil is expressed as:

$$K(s_e) = \left(s_e^{\frac{1}{2}} \left[1 - \left(1 - s_e^{\frac{1}{m}} \right)^m \right]^2 \right) K_s \tag{3.4}$$

Uncertainty in the SWRC has been relatively well-studied in geotechnical engineering (e.g., Gitirna and Fredlund 2005; Phoon et al. 2010; Chiu et al. 2012; Tan et al. 2013; Zhang and Yan 2015). Phoon et al. (2010) studied the probabilistic analysis of SWRC by casting a probability model for curve fitting parameters (α_V, n). Their study covered sandy clay loam, loam, loamy sand, clay, and silty clay data in Unsaturated Soil Hydraulic Database (UNSODA). Moreover, they state that θ_s is fixed at the experimental value related to zero suction which means θ_s is not a fitting parameter. On the other hand, they showed that different assumptions on the residual water content (e.g., $\theta_r = 0$ or $\theta_r \neq 0$) lead to different SWRC curves over the high suction rage. Since only a few data points in the database present high suction range, they concluded that it is very difficult to present which assumption is more accurate (Phoon et al. 2010). Subsequently, they limited their statistical study to α_V and n. For the same reason this study only considerers α_V and n as fitting parameters for RIGA.

Phoon et al. (2010) found the correlation between α_V, n with a maximum correlation coefficient reported as -0.487 for clay. They used a lognormal joint probability model to represent point variability of SWRC. In this study, the same approach is used but the proposed joint distribution function will be extended for $\alpha_V, n,$ and K_s.

3.2.2.1 Database of unsaturated hydraulic properties

In this study, data is extracted from UNSODA which was developed by U.S. Salinity Laboratory, U.S. Department of Agriculture (Leij et al. 1996). The database includes test results of hydraulic properties from 780 unsaturated soils ranging from clays to sand. In the current study, α_V, n and K_s are considered as Random Variables (RVs). The test results for silty loam and sandy loam from UNSODA are used to characterize the variability of $\alpha_V, n,$ and K_s. In order to find the joint distribution function of RVs, the test records such as suction, moisture content, and saturated hydraulic conductivity for silty loam and sandy loam samples are obtained. The fitting parameters $\alpha_V,$ and n are then determined using the constrained non-linear optimization method. This method finds a vector that is a local minimum to a scalar function subjected to constraints on the permissible vector. This procedure is accomplished using the built in subroutine "*fmincon*" in Matlab8.1 (R2013a). After discarding incomplete data and excluding outliers, 48 and 40 data sets were used for silty loam and sandy loam, respectively.

3.2.2.2 Statistical distribution of hydraulic properties

From a material properties point view, PDFs with non-negative values (e.g., exponential, Weibull, and lognormal distribution) are preferred to define the probability distribution of RVs as these properties are typically positive. Specifically, the lognormal PDF has been successfully used in a variety of analyses, including unsaturated soils (e.g., Babu and Murthy, 2005; Likos et al., 2013; Tan et al. 2013). Griffiths and Fenton (1993) used a lognormal distribution of K_s to model the random field in steady-saturated seepage problems using their proposed Random FEM (RFEM) framework. In addition,

Phoon et al. (2010) showed that the distributions of α_V and n also follow a lognormal PDF.

We performed our statistical analysis based on the assumption of a joint lognormal distribution of α_V, n and K_s for silty loam and sandy loam. Since all three RVs are continuous, the fitness of the proposed PDF is tested by Anderson Darling (AD) criteria (Fenton and Griffiths, 2008). A given set of RVs (Y) is lognormally distributed if $ln(Y)$ follows a normal distribution. Consequently, the PDF for the random variable (y) is defined:

$$f_Y(y) = \frac{1}{(y-A)\sigma_{lnY}\sqrt{2\pi}} exp\left(-\frac{1}{2}\left(\frac{ln(y-A)-\mu_{lnY}}{\sigma_{lnY}}\right)^2\right) , \qquad y > A \tag{3.5}$$

where μ_{lnY} and σ_{lnY} are mean and standard deviation of the corresponding normal distribution, respectively, and A defines the threshold where the Cumulative Distribution Function (CDF) of Y is zero below that. A is defined based on practical cases, which matches the physics of problem. The values of A for $K_s, \alpha_V,$ and n are (0,0,1), respectively. The mean and variance of y are obtained by using the moment generating function of lognormal RV. The transformation between the mean and variance of a lognormal distributed RV and corresponding normal distribution are defined as:

$$\mu_{lnY} = ln(\mu - A) - \frac{1}{2}{\sigma_{lnY}}^2 \tag{3.6}$$

$${\sigma_{lnY}}^2 = ln\left(1 + \frac{\sigma^2}{(\mu-A)^2}\right) \tag{3.7}$$

where μ and σ are the mean and standard deviation of measured data, respectively. These parameters can be estimated by sample mean and standard deviation ($\mu \cong \overline{\mu} = \frac{\sum y}{N}$, $\sigma \cong \overline{\sigma} = \left(\frac{\sum(y-\overline{\mu})^2}{N-1}\right)^{1/2}$, N represents the sample size). In addition, the

requirement for introducing a joint PDF is considered based on a linear correlation between normal RVs. Phoon (2004) introduced a closed-form equation that relates the correlation of normal random vectors $ln(Y_i)$ and $ln(Y_j)$ ($\rho_{lnY_i lnY_j}$) to the correlation of the corresponding lognormal vectors Y_i and Y_j ($\rho_{Y_i Y_j}$):

$$\rho_{Y_i Y_j} = \frac{exp\left(\sigma_{lnY_i}\sigma_{lnY_j}\rho_{lnY_i lnY_j}\right)-1}{\sqrt{\left(exp\left(\sigma_{lnY_i}{}^2\right)-1\right)\left(exp\left(\sigma_{lnY_j}{}^2\right)-1\right)}} \tag{3.8}$$

Table 3.1 shows linear correlation ($\rho_{lnY_i lnY_j}$), mean ($\overline{\mu}$), standard deviation ($\overline{\sigma}$), coefficient of variation (cov) for the silty loam and sandy loam sampels which were used in this study. The statistical correlation between the three parameters can be explained by the relation between physical factors controlling these variables. As noted before, α_V and *n* approximate the inverse of air entry value and pore size distribution, respectively. The air entry value is directly connected to the characteristics of soil pore size distribution. The pore size distribution depends on the particle size distribution, the particles arrangement and the soil composition among others. Saturated hydraulic conductivity closely correlated to soil texture, particle size distribution and soil bulk density.

Table 3.1 Statistical analysis of silty loam and sandy loam samples used in this study.

	Silty Loam				Sandy Loam		
$\rho_{lnY_i lnY_j}$	Ks(m/s)	α(1/m)	n	$\rho_{lnY_i lnY_j}$	Ks(m/s)	α(1/m)	n
Ks (m/s)	1	-0.06	0.01	Ks (m/s)	1	0.25	0.11
α_V (1/m)	-0.06	1	-0.32	α_V (1/m)	0.25	1	-0.44
N	0.01	-0.32	1	n	0.11	-0.44	1

$\overline{\mu}$	4.84e-6	1.04	1.36	$\overline{\mu}$	9.57e-6	2.62	1.33
$\overline{\sigma}$	5.48e-6	1.06	1.95	$\overline{\sigma}$	2.40e-5	3.49	0.16
cov	1.13	1.02	0.14	cov	2.51	1.33	0.12

In the above definition, lognormal random vector $Y_i(i = 1,2,3)$ represents K_s, α_V, and n, respectively. It is noted that the subscript i is not represented in the next sections for simplicity.

Figures 3.1 and 3.2 show the histograms and estimated PDFs for K_s, α_V, and n for silty loam and sandy loam, respectively. In all figures, the frequency of occurrence in each bin is normalized by the total number of data points with respect to the given data set. The probability of mistakenly rejecting the lognormal hypothesis is defined by significance level of 5%. The AD goodness-of fit test indicates that the lognormal distribution is acceptable to represent the PDF for the RVs of interest. The minimum significance level (*P_value* = 0.135) is observed for the data representing n in silty loam (Figure 3.1(c)). It still shows that the hypothesis of representing lognormal distribution is valid for n.

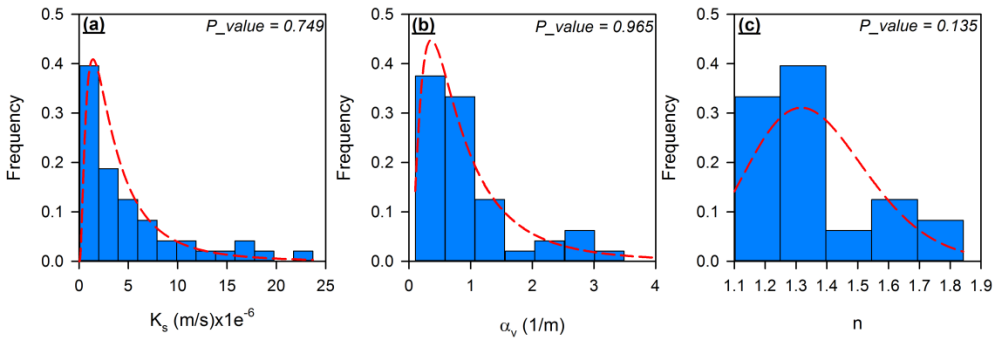

Figure 3.1 Statistical analysis for silty loam: (a) Histogram and estimated PDF for K_s. (b) Histogram and estimated PDF for α_V. (c) Histogram and estimated PDF for n.

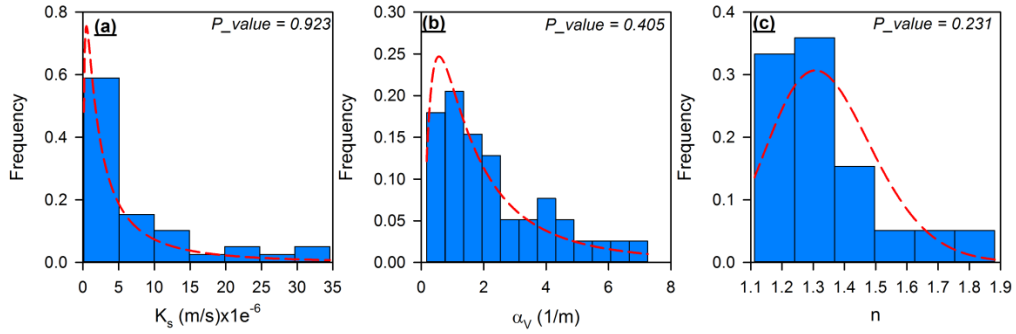

Figure 3.2 Statistical analysis for sandy loam: (a) Histogram and estimated PDF for K_s. (b) Histogram and estimated PDF for α_V. (c) Histogram and estimated PDF for n.

3.2.3 Spatial Variability

In the previous section, we considered the variability of quantities at a point in a given medium. In this section, we add the spatial variability of RVs in the domain and study the possible correlations between them. Spatial dependence between two positions, t^* and t', is negatively dependent on the distance between these two points ($\tau = t^* - t'$). For instance, two RVs, $ln\, Y(t^*)$ and $lnY(t')$, are statistically more likely to be similar, or

correlated, when τ is small and dissimilar, or uncorrelated, when τ is large (Fenton and Griffiths, 2008). The spatial dependency results in smoothing of random process; however, including all points in this scheme leads to a joint PDF with infinite dimensions. Assumptions of statistical homogeneity and isotropy can be used to alleviate this problem. Statistical homogeneity implies that the joint PDF is independent of spatial position and depends only on relative positions of the points in a given domain. This indicates that the mean, variance, and higher order moments are constant in space. In addition, isotropy suggests that the joint PDF is invariant under rotation, which indicates that the correlation between two points only depends on the distance between them and is independent from their orientation relative to one another in two- or three-dimensional random fields (Fenton and Griffiths, 2008).

Since the RVs are Gaussian and stationary, we only need the following items to characterize them:

1) Mean μ_{lnY}.

2) Variance ${\sigma_{lnY}}^2$.

3) Point correlation $\rho_{lnY_i lnY_j}$.

4) How rapidly the RVs vary in space.

Items 1, 2 and 3 have been considered in the previous section, while the last is discussed in the rest of this section. The rate of variation of RVs in space is based on the second moment of the joint PDF. The covariance function, spectral density function, and variance function are equivalent to the second moment of the joint PDF. In this study, we use covariance and variance functions to capture the spatial variability of the RVs.

The covariance function defines the second moment for joint Gaussian RVs. Since lnY is stationary, μ_{lnY} and σ_{lnY} are independent of position, consequently, the covariance function can be expressed just in term of τ:

$$Cov(lnY(t^*), lnY(t')) = Cov(lnY(t), lnY(t+\tau)) = Cov(lnY(0), lnY(\tau)) = C(\tau) \quad (3.9)$$

The covariance function $C(\tau)$ generates a positive definite set if we consider the covariance matrix $\boldsymbol{C} = [C(\tau)_{ab}]$, where a and b show two different positions in a given domain. The square root of $\boldsymbol{C}$ is real and equals the lower triangular matrix L_c, which is obtained by Cholesky decomposition (Griffiths and Fenton, 2007):

$$\boldsymbol{C} = L_c \times {L_c}^T \quad (3.10)$$

Since the magnitude of covariance depends on the size of the RVs, it does not give much information about linear dependence between random fields. Subsequently, a more meaningful measure is to study the dependency/independency of RVs by the correlation function:

$$\rho_s\big((lnY(t^*), lnY(t')\big) = \frac{C(\tau)}{{\sigma_{lnY}}^2} \quad (3.11)$$

where ρ_s shows the spatial correlation between RVs. In this study, we used the Markov correlation function for simplicity:

$$\rho_s(\tau, \varepsilon) = exp\left(-\frac{2|\tau|}{\varepsilon}\right) \quad (3.12)$$

where ε is the correlation length; ε indicates the spatial domain of RVs where beyond that the RVs are largely uncorrelated (see Figure 3.3).

In practice, common engineering properties represent the local average over the laboratory samples. For instance, failure load is defined as the average of bond strength over the failure region (Fenton and Griffiths, 2008). This idea is also used in the study of

behavior of random fields over the area (A) of a given 2D domain with length T_1 and T_2 ($A = T_1 \times T_2$).

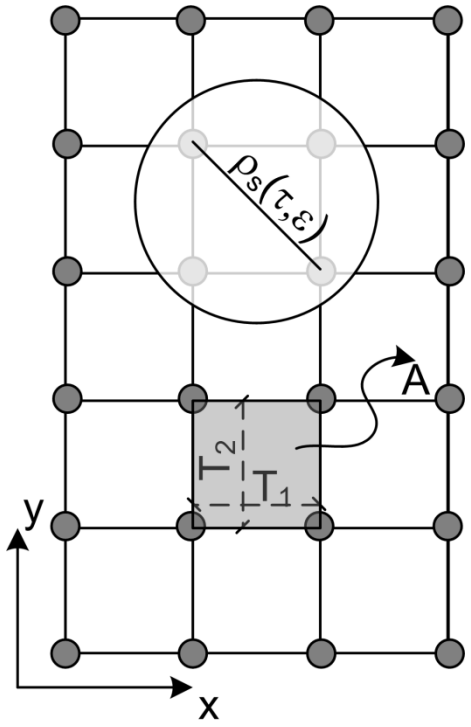

Figure 3.3 Spatial correlation $\rho_s(\tau, \varepsilon)$ and arithmetic average of random fields over $A = T_1 \times T_2$.

Fenton and Griffiths (2008) show that the local arithmetic averaging preserves the mean of the random field while variance in random fields decreases by a reduction factor (γ):

$$\gamma(T_1, T_2) = \frac{4}{T_1^2 T_2^2} \int_0^{T_1} \int_0^{T_2} (|T_1| - \tau_1)\,(|T_2| - \tau_2) \rho_s(\tau) d_{\tau_1} d_{\tau_2} \tag{3.13}$$

where $|\tau| = \sqrt{\tau_1^2 + \tau_2^2}$ in two-dimensional (2D) geometry.

3.2.4 Random Isogeometric analysis

This study uses IGA in a non-deterministic way by combining it with random fields. Here, it is tried to solve Richards' equation with respect to uncertainty and randomness in soil properties. The numerical solution follows exactly Chapter 2 and we just focus on probabilistic analysis in the rest of thesis.

3.2.5 RIGA Solution Procedure

The analysis of unsaturated flow for a given realization using RIGA is described in the following steps with respect to point and spatial variability of unsaturated soil properties:

0. Discretize the problem geometry using IGA.

1. Generate three uncorrelated standard normal random samples with respect to number of nodes ($nNodes$) in the discretized domain. $U = [U_1, U_2, U_3]_{nNodes\times 3}$. Since the sample mean can be non-zero for small sample sizes, the sample mean is removed from the simulated numbers. This procedure is done by built in subroutine "randn" in Matlab8.1 (R2013a).

2. Calculate the covariance matrix for U and imply Cholesky decomposition to find lower triangular matrix $[L_U]_{3\times 3}$.

3. Find correlation matrix for normally distributed data (Eq. (3.8)) and imply Cholesky decomposition to find lower triangular matrix $[L_{lny}]_{3\times 3}$.

4. The correlated normal random vector is generated using the Cholesky factor of the correlation matrix. $[X]_{nNodes\times 3} = U \times (L_{lny} \times {L_U}^{-1})^T$.

5. Generate spatial correlated random fields with respect to X by Eq. (3.12). Then calculate the lower triangular matrix $[L_c]_{nNodes \times nNodes}$ using Eq. (3.10).

6. Generate spatially correlated normal random vector using $[S_n]_{nNodes \times 3} = L_c \times X$.

7. Average S_n over the discretized domain (elements) and calculate covariance reduction factor γ_e $(e = 1 \dots number\ of\ elements)$ regarding the size of elements using Eq. (3.13).

8. The correlated lognormal random vectors $Y_{ei}(i = 1,2,3)$ which show the elements properties are defined as $Y_{ei} = exp(\overline{\mu}_i + {\gamma_e}^{0.5}\overline{\sigma}_i\, S_{n_i}) + A_i$ ($\overline{\sigma}_i\, S_{n_i}$ does not represent the indicial summation).

9. Continue the realization via IGA using elements properties introduced in step 8.

Performing Monte Carlo simulation using adequate numbers of realizations (following steps: 0-9) leads to RIGA analysis of unsaturated flow in porous media, considering the point and spatial variability of hydraulic properties. It is noted the algorithm presented by Phoon (2004) is used in the current study to generate correlated and lognormal distributed RVs. This procedure simulates uncorrelated standard normal RVs and transforms them into correlated normal RVs with the appropriate correlation formula introduced by Eq. (3.8) and finally, translates the correlated normal to correlated lognormal RVs.

3.3 Example Problems

Two sets of results are usually of particular interest in unsaturated flow problems: a) pore water pressure distribution, and b) inflow and outflows. The following sections

present two example problems to demonstrate the application of RIGA for investigating the aforementioned set of results. The first example problem involves one-dimensional unsaturated flow in a rectangular domain. In this example, we employed RIGA to explain how the outflow varies with inherent uncertainties in soil properties. In the second example, unsaturated flow in a two-dimensional furrow, we show that how the random nature of soil affects the pore water pressure distribution and how the probabilistic solution is different from a deterministic scenario.

3.3.1 One-dimensional unsaturated flow in a rectangular domain

The first example problem represents a rectangular domain (W X L) consisting of silty loam. In this problem the effect of ε and geometry ratio (W/L) on the outflow (Q) from bottom boundary is studied. The boundary conditions on the top and bottom of the domain are Dirichlet boundary conditions (Γ_D). The top boundary is subjected to a constant head of 2 m and the bottom boundary is located on the water table. According to Figure 3.4(a), the datum is defined on the soil surface, which introduces a constant head – L on the bottom boundary. Based on the defined boundary conditions, this problem represents a one-dimensional (1D) flow in a 2D geometry.

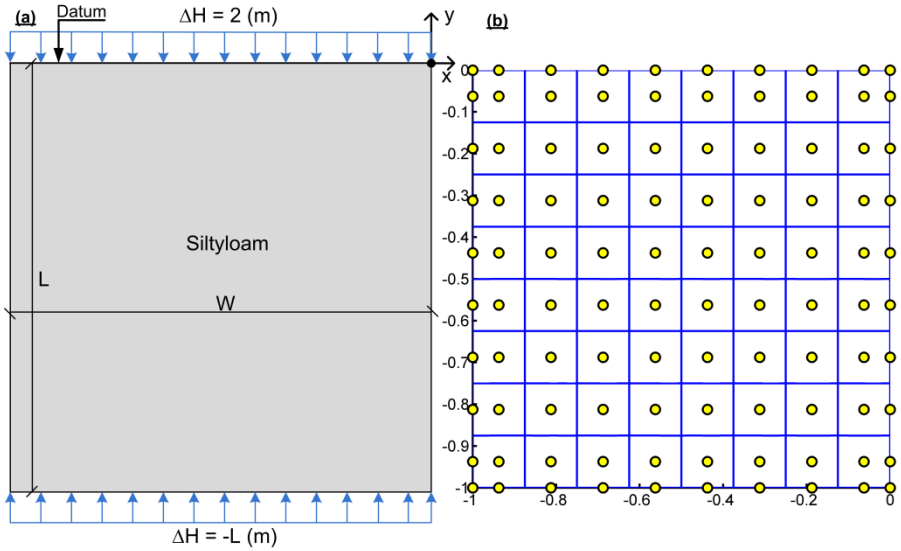

Figure 3.4 (a): Rectangular domain representing 1D flow in silty loam. (b): Discretized domain using 100 DOFs.

The problem domain is discretized using elements in IGA. The order of approximation is p = q = 2 and the corresponding knot vectors and control points are defined as:

$$\xi = \eta = \{0\ 0\ 0\ 1\ 1\ 1\} \tag{3.14}$$

$$P_{ij} = \begin{Bmatrix} 0 & -0.5 & -1 & 0 & -0.5 & -1 & 0 & -0.5 & -1 \\ 0 & 0 & 0 & -0.5L & -0.5L & -0.5L & -L & -L & -L \end{Bmatrix}$$

The corresponding weight vector is unit in this problem. For illustrative purposes, Figure 3.4(b) represents the discretized domain using 100 DOFs and quadratic elements for the geometry ratio W/L=1. To achieve a computationally accurate solution the DOF were increased from 100 to 1156 for Monte Carlo simulations, In order to study the effect of geometry on the outflow distribution at the bottom boundary, three geometry ratios (W/L= 1/6, 1, and 6) are studied. The correlation length varies with respect to ε = [0.005, 0.05, 0.25, 0.5, 1, 1.5] m for a given geometry ratio. For each individual ε, 1000 Monte

Carlo simulations were performed and the corresponding Q at the bottom boundary was recorded. The number of realizations is problem-specific and was determinate through a sensitivity analysis. For this problem, it was found that the changes in mean and standard deviation were negligible beyond 1000 realizations.

Figure 3.5 shows the dependency of coefficient of variation (COV) of outflow in steady sate conditions on the correlation length. It is observed in Figure 3.5 that dependency of COV exponentially increases as the correlation length grows. It is also shown in Figure 3.5 that by increasing W/L the COV of results from Monte Carlo simulations increases. Figure 3.5 suggests that the variation in the simulations is considerable as the distance between the water table and soil surface decreases for $\varepsilon \geq 0.1\text{m}$.

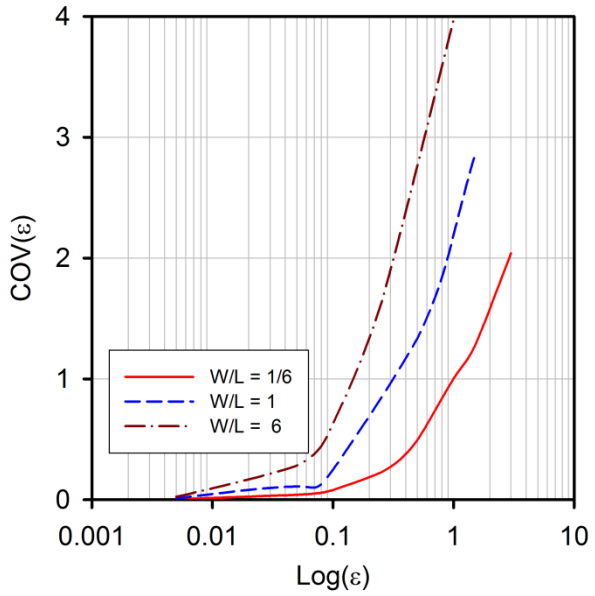

Figure 3.5 Dependency of coefficient of variation on correlation length in Monte Carlo simulations.

In order to study the effect of ε on the results, the outflow variation with respect to $\varepsilon = 0.05, 0.25$, and 0.50 m is studied in the proposed geometry ratios. The frequency of occurrence is normalized by the total number of simulations in each bin and it is assumed that in all analyses, the lognormal distribution is the null hypothesis to represent the PDF for Q. The goodness of fit test (AD) suggests that the lognormal distribution is acceptable with a significance level of 5% in all cases. Higher P_values show more confidence in representing the distribution of Q with a lognormal function. The increase in COV as ε increases is captured in Figure 3.6 for W/L=1/6. In addition, the histograms for values of Q are shown to be slightly skewed to the left as ε increases. The minimum P_value is observed for $\varepsilon = 0.5$ m while the maximum P_value is observed for $\varepsilon = 0.05$ m.

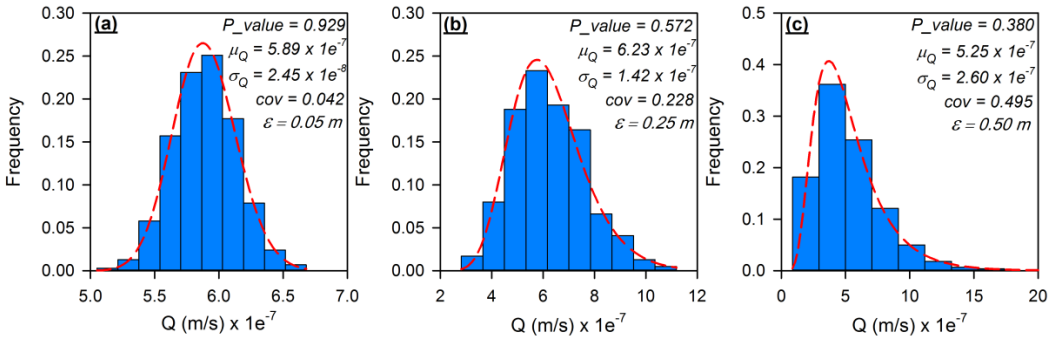

Figure 3.6 Lognormal PDF of Q in geometry ratio (W/L=1/6): (a) correlation length $\varepsilon = 0.05$. (b) correlation length $\varepsilon = 0.25$. (c) correlation length $\varepsilon = 0.50$ m.

Increase in the geometry ratio (W/L) from 1/6 to 1 leads to an increase in Q for all ε values, as shown in Figure 3.7. In addition, Figure 3.7 shows that higher ε leads to higher COV, similar to the trend seen for the ratio W/L=1/6. The histograms show that an

increase in ε results in data that is more skewed to lower values of Q and covers wider ranges than smaller values of ε.

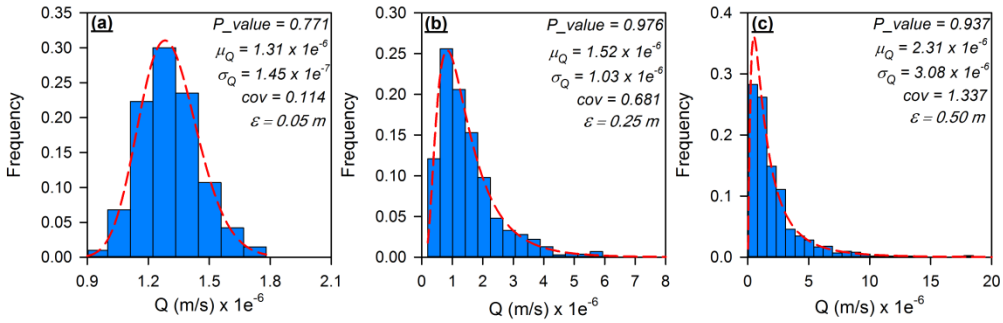

Figure 3.7 Lognormal PDF of Q in geometry ratio (W/L=1): (a) correlation length ε = 0.05. (b) correlation length ε = 0.25. (c) correlation length ε = 0.50 m.

The last scenario in the parametric study deals with the geometry ratio W/L = 6. Similar to the trend seen in Figures 3.6 and 3.7, the COV increases as ε grows. However, the rate of change in COV is intensified with respect to increase in the geometry ratio. For instance, Figures. 3.6, 3.7, and 3.8(c) show that by increasing W/L the COV considerably increases from Q = 0-20 x $1e^{-7}$ m/s (Figure 3.6(c)) to 0-140 x $1e^{-6}$ m/s (Figure 3.8(c)). Subsequently, changes in W/L lead to variation in COV from 0.495 to 2.107.

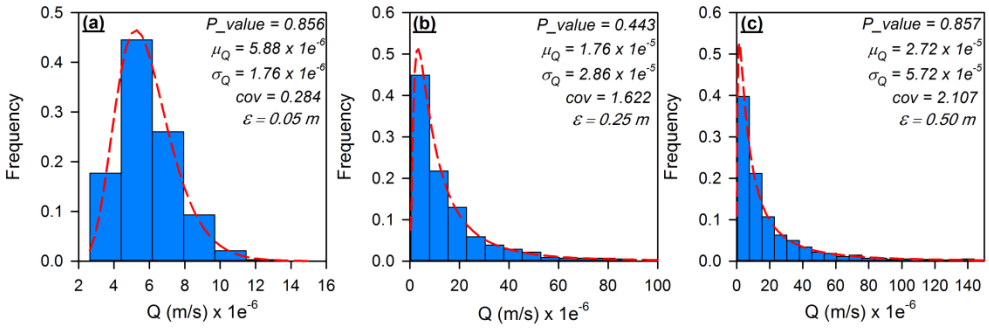

Figure 3.8 Lognormal PDF of Q with geometry ratio (W/L=6): (a) correlation length $\varepsilon = 0.05$. (b) correlation length $\varepsilon = 0.25$. (c) correlation length $\varepsilon = 0.50$ m.

3.3.2 Two-dimensional Furrow problem

In the second example, RIGA is used to model an infiltration problem in a semi-circular furrow. This problem includes a 2D flow in a variably saturated soil. Due to symmetry, only half of the problem is considered with Sandy-loam properties (Table 3.1). Figure 3.9(a) shows an unsaturated domain subjected to infiltration rate of $q/K_{s(mean)} = 0.5$ in the circular geometry while the bottom boundary sits on the water table. The prescribed head on the bottom boundary is constant (h = -4m) and $K_{s(mean)}$ represents the mean value of saturated permeability for sandy loam. In order to represent the problem in IGA, bi-quadratic elements are used to discretize the geometry. The associated knot vectors with respect to each direction are defined as $\boldsymbol{\Theta}(\xi)_r = \{0, 0, 0, 0.5, 1, 1, 1\}$ and $\boldsymbol{\Theta}(\xi)_t = \{0, 0, 0, 1, 1, 1, 1\}$ where *r* and *t* represent the discretization directions (Figure 3.9(b)). The corresponding control points with respect to $\boldsymbol{\Theta}(\eta)_r$ and $\boldsymbol{\Theta}(\xi)_t$ are defined as:

$$\boldsymbol{P}_{i,j} = \begin{Bmatrix} 0 & -0.4142 & -1 & -1 & 0 & -0.75 & -2.5 & -2.5 & 0 & -3.99 & -4 & -4 \\ -1 & -1 & -0.4142 & 0 & -2.5 & -2.5 & -0.75 & 0 & -4 & -4 & -4 & 0 \end{Bmatrix} \quad (3.15)$$

To accurately simulate the semi-circle geometry at the top boundary, the following weight vector for associated control points is defined as:

$$w_i = \left\{1 \quad 1+\frac{1}{\sqrt{2}} \quad 1+\frac{1}{\sqrt{2}} \quad 1 \quad 1 \quad 1 \quad 1 \quad 1 \quad 1 \quad 1 \quad 1\right\} \tag{3.16}$$

For illustration purpose, Figure 3.9(b) shows the discretized domain with 165 DOFs while in order to obtain accurate results, the Monte Carlo simulation is performed using 612 DOFs.

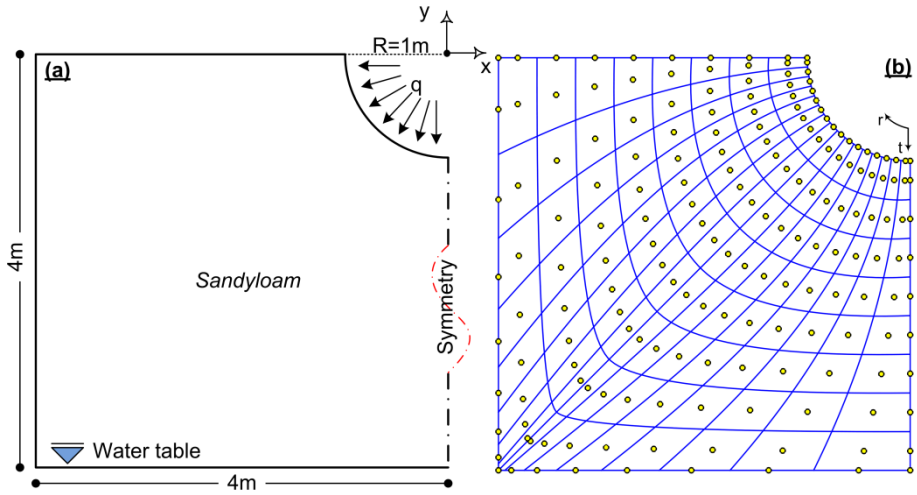

Figure 3.9 Infiltration problem in semi-circular furrow: (a) Geometry and hydraulic boundary conditions. (b) Discretized domain using quadratic IGA mesh.

Monte Carlo simulation includes 1500 realizations to represent the random nature of HCF in this problem. For this problem, the changes in mean and standard deviation were found to be negligible beyond 1500 realizations. Figures 3.10 and 3.11 show three realizations and associated results in steady state conditions with the aim of representing averaged K_s in the IGA elements. The outcomes from Figure 3.10 correspond to a lognormal random vector for point and spatial variability. The color code in the

discretized domain shows lower permeability in the darker elements and higher permeability in the lighter ones and Figure 3.11 shows the corresponding head contours in the same realizations. Figures 3.10 and 3.11 illustrate that the effects of random properties on unsaturated seepage analysis. It is seen that the variation in pore pressure increases in the regions with lower permeability blocks. Unlike the deterministic analysis (Figure 3.12(a)), the pore pressure profile is not smooth and due to the random nature of unsaturated soil hydraulic properties, the pore pressure profile is not unique and varies in each realization with respect to different elements' properties.

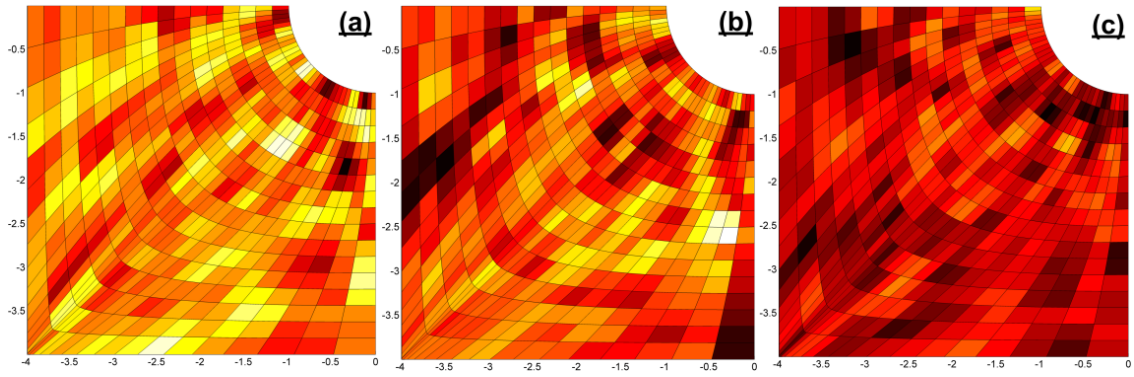

Figure 3.10 Random field (K_s) representation in IGA elements in three realizations.

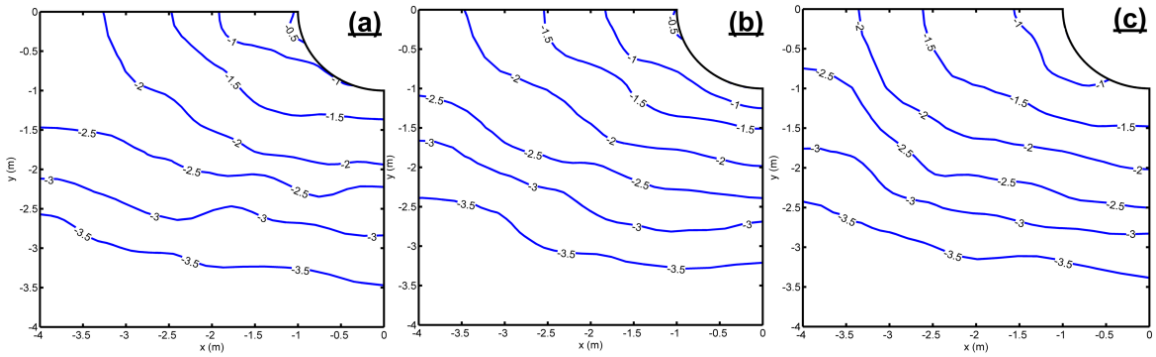

Figure 3.11 Head contours in three different realizations.

The outcomes of 1500 simulations are compared with deterministic results including $\bar{\mu}$ for K_s, α_V, and n (sandy loam in Table 3.1). Figure 3.12(a) represents the head values in the probabilistic and deterministic approach. The probabilistic approach includes the mean of 1500 realizations while the deterministic results are obtained directly from the problem simulation with $\bar{\mu}$ for K_s, α_V, and n. It is observed that the difference between the probabilistic and deterministic analyses is considerable in unsaturated flow simulations.

Figure 3.12(b) shows the standard deviation of the results from the Monte Carlo simulations. The results from the simulations show that standard deviation values vary from the minimum 0.02 m to the maximum 0.18 m in the problem domain. The minimum values of standard deviation are close the bottom boundary since the value of total head is constant on this boundary. Analogous to the previous example with a geometry ratio W/L = 1/6, the standard deviation of the results decreases as the distance between the water table and soil surface increases.

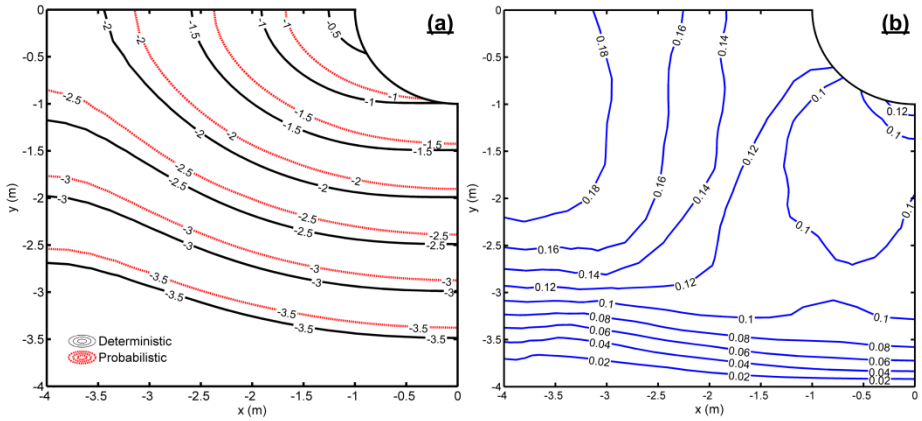

Figure 3.12 (a) Difference between the mean of 1500 Monte Carlo realizations and results from deterministic solution, (b) standard deviation in the results of 1500 simulation.

Equation (3.13), along with step 7 in the RIGA solution procedure, indicates that the covariance reduction factor (γ_e) should be considered for obtaining the average of an element's properties over the discretized domain. Figure 3.13 shows the color codes that represent changes in γ_e within the discretized domain. Figure 3.13 indicates that γ_e increases as the element size decreases. The minimum value for γ_e is observed as 0.5 and the maximum value of γ_e is 0.75 in the discretized domain. While beyond the scope of this study, the results obtained from RIGA can also be employed to determine the probability of occurrence of a specified event, such as the resulted water head in this example problem.

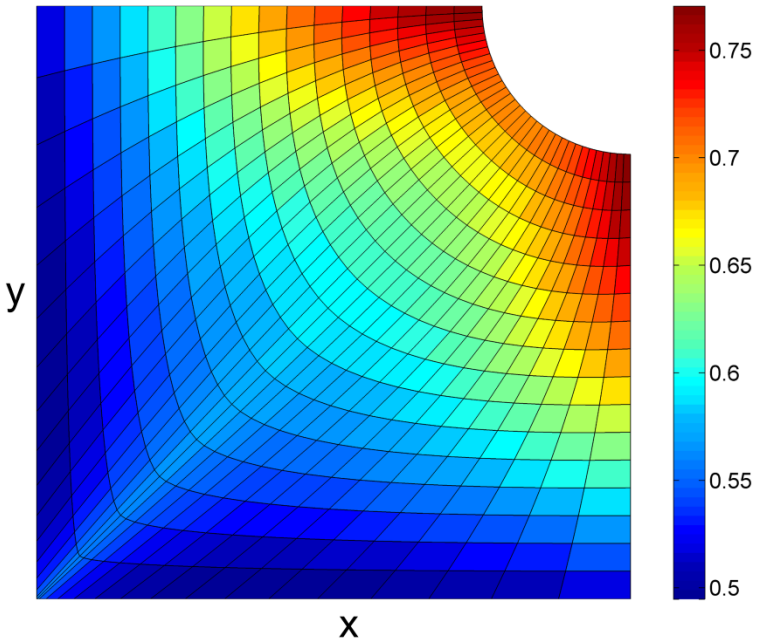

Figure 3.13 Covariance reduction factor (γ_e) in the discretized domain with quadratic IGA elements.

CHAPTER IV

CONCLUSION

4.1 Summary of work accomplished for head-based Isogeometric analysis of transient flow in unsaturated soils

This part of the study presented a head-based IGA solution for transient flow in heterogeneous unsaturated soils. In general, the proposed IGA uses NURBS basis functions to approximate geometry and field variables, a feature which provides accurate results and an easier mesh generation/refinement procedure. The results from the proposed IGA formulation were validated and compared against analytical solution and conventional FEM. The IGA results, with different orders of approximations were found in good agreement with analytical solutions for 1D and 2D problems in one- and two-layer soil systems. The utilization of NURBS basis functions leads to higher-order accurate results in the h-based solution. In addition, the intrinsic property of c^0 NURBS basis functions allows defining the soil internal boundaries with local mesh refinement. These features of the proposed IGA method provide better performance in heterogeneous unsaturated mediums and problems with complex geometries and allow precise tracking of the water front at the intersection of the soil layers. Regarding mass lumping, the row-sum technique was used for IGA and linear FEM simulations while special mass-lumping technique was utilized in quadratic FEM simulations. The rate of convergence for both

IGA and FEM models is found identical. However, in highly nonlinear unsaturated problems, the application of quadratic FEM is limited whereas higher order IGA simulations are applicable. Moreover, the comparison of results between quadratic IGA and FEM shows that the IGA framework obtains closer results to analytical solutions where hydraulic conductivity is high. Moreover, it is noted that the computational costs are considerably reduced if adaptive time steps are used in the solution framework.

4.2 Summary of work accomplished for random Isogeometric analysis (RIGA) for modeling seepage in unsaturated soils

Since modeling seepage problems in unsaturated soils involve various uncertainties owning to the random nature and variability of unsaturated soil properties, In the third chapter, we considered the point and spatial variability of unsaturated flow in porous media in the formulation of a new numerical scheme called Random Isogeometric analysis (RIGA). The proposed probabilistic framework can be easily extended to analysis of problems governed by partial differential equations, including uncertainty in various fields (e.g., geotechnical, petroleum, and agricultural engineering). To illustrate the application of the proposed method, RIGA is implemented in the analysis of uncertainty in unsaturated flow problems. K_s, α_V, and n are considered as three random variables (RVs) in this study. It is shown that correlated lognormal probability distribution function (PDF) is the appropriate distribution function to represent point variability of the RVs. Regarding the analysis of spatial variability of random fields, the Markov correlation function is studied and it is observed that the covariance of results from Monte Carlo simulation is an exponential function of correlation length and geometry ratios. Furthermore, it was found that the outflow probability distribution also

follows a lognormal PDF. It is observed that the outflow PDF is skewed to lower values of flow as the correlation length and geometry ratio increases. In addition, the analysis showed that the variability in results is a function of the vadose zone length. The increase in vadose zone length leads to less variation in outflow. The results from RIGA were compared against a deterministic solution and considerable differences were found between the probabilistic and deterministic analyses. The proposed framework offers a robust and computationally efficient means for probabilistic investigation of pore water pressure distribution and flow quantities in unsaturated earthen structures such as slopes, dams, levees, sheet piles. Further, properly accounting for the variability of unsaturated soil properties leads to more realistic estimations of suction, a critical factor that can significantly affect the serviceability and stability of earthen structures subjected to steady and transient unsaturated flows.

4.3 Recommendation for future works

In this research, the performance of IGA in solving unsaturated seepage problems was evaluated. Further, a probabilistic IGA-based framework, RIGA, was developed to consider the randomness and uncertainty of unsaturated soil hydraulic properties in the analysis. This research considered a single-phase flow and assumed that the gas phase is constant at the atmospheric level. In addition, the density of fluid was taken constant during the analysis and no interaction was considered between solid particles and water constituent.

For future research, the proposed IGA modeling of unsaturated flow can be further extended through one or combination of the following:

- Simulating a more general case of two-phase flow where both water and air pressures exists and are treated as unknown variables in the analysis.
- Developing a fully coupled model for the analysis of water and airflow in deforming porous media in variably saturated conditions. For this purpose, the solid displacements and the pressures of fluids can be taken as primary unknowns of the simulation.
- Considering the fact that the density of fluid is not often uniform and it can be influenced by variations in temperature and pressure. The increase in temperature leads to decrease in density while the increase in pressure leads to increase in density and vice versa. The fluid density should be considered as a dependent thermodynamic variable where its spatial and temporal variations play a key role in variable-density flow problems.
- Developing fully coupled numerical model to simulate the unsaturated transient flow including heat and mass transfer in deforming porous media by taking into account the incompressibility of fluid. In this case, the governing equations in terms of displacement, temperature, capillary pressure, and gas pressure are coupled and form a nonlinear system of differential equations that will be solved by the proposed IGA framework.

REFERENCES

Arampatzis, G., (2000). "Experimental research on wetting and drainage to layered soils. Simulation with the method of finite volume" (Doctoral dissertation, PhD thesis, Aristotle University of Thessaloniki).

Ashcroft, G., Marsh, D.D., Evans, D.D. and Boersma, L., (1962). "Numerical method for solving the diffusion equation: I. Horizontal flow in semi-infinite media". Soil. Sci. Soc. Am. J, 26(6), pp.522-525.

Ashcroft, G., Marsh, D.D., Evans, D.D. and Boersma, L., (1962). "Numerical method for solving the diffusion equation: I. Horizontal flow in semi-infinite media". Soil Sci.Soc. Am. J., 26(6), pp.522-525.

Bastani, A.F. and Damircheli, D., (2017). "An adaptive algorithm for solving stochastic multi-point boundary value problems". *Num. Alg.*, *74*(4), pp.1119-1143.

Bastani, A.F. and Damircheli, D., (2013). "On Adaptive Multiple-Shooting Method for Stochastic Multi-Point Boundary Value Problems". arXiv:1301.4774.

Bazilevs, Y., Calo, V.M., Zhang, Y. and Hughes, T.J., (2006). "Isogeometric fluid–structure interaction analysis with applications to arterial blood flow". Comput. Mech., 38(4-5), pp.310-322.

Broadbridge, P. and White, I., (1988). "Constant rate rainfall infiltration: A versatile nonlinear model: 1. Analytic solution". Water Res. Res., 24(1), pp.145-154.

Brooks, R. H., Corey, A. T. (1964). "Hydraulic properties of porous media and their relation to drainage design". Trans. ASAE, 7(1), 26-0028.

Brunone, B., Ferrante, M., Romano, N. and Santini, A., (2003). "Numerical simulations of one-dimensional infiltration into layered soils with the Richards equation using different estimates of the interlayer conductivity". Vadose Zone Journal, 2(2), pp.193-200.

Celia, M.A., Bouloutas, E.T. and Zarba, R.L., (1990). "A general mass- conservative numerical solution for the unsaturated flow equation". Water Res. Res., 26(7), pp.1483-1496.

Cheng, Y., Zhang, L. L., Li, J. H., Zhang, L. M., Wang, J. H., & Wang, D. Y. (2016). "Consolidation in spatially random unsaturated soils based on coupled flow-deformation simulation". Int. J. Num. Anal. Meth. Geomech. DOI: 10.1002/nag.2572.

Chiu, C. F., Yan, W. M., & Yuen, K. V. (2012). “Reliability analysis of soil–water characteristics curve and its application to slope stability analysis”. Eng. Geology, 135, 83-91.

De Boor, C., (1972). “On calculating with B-splines”. J Approx Theory, 6(1), pp.50-62.

Diersch, H.J. and Perrochet, P., (1999). “On the primary variable switching technique for simulating unsaturated–saturated flows”. Adv. Water Res., 23(3), pp.271-301.

Diersch, H.J.G., (2013). “FEFLOW: finite element modeling of flow, mass and heat transport in porous and fractured media”. Springer Science & Business Media.

Elkateb, T., Chalaturnyk, R., & Robertson, P. K. (2003). “An overview of soil heterogeneity: quantification and implications on geotechnical field problems”. Canad. Geotech. J., 40(1), 1-15.

Fenton, G. A., Griffiths, D. V. (2003). Bearing-capacity prediction of spatially random c-φ soils. Canadian Geotechnical Journal, 40(1), 54-65.

Fenton, G. A., Griffiths, D. V. (2008). “Risk assessment in geotechnical engineering”. Wiley.

Forsyth, P.A., Wu, Y.S. and Pruess, K., (1995). “Robust numerical methods for saturated-unsaturated flow with dry initial conditions in heterogeneous media”. Adv. Water Res., 18(1), pp.25-38.

Fredlund, D. G., Xing, A. (1994). “Equations for the soil-water characteristic curve”. Canad. Geotech. J, 31(4), 521-532.

Gardner, W.R., (1958). “Some steady-state solutions of the unsaturated moisture flow equation with application to evaporation from a water table”. Soil Sci., 85(4), pp.228-232.

Gitirana J. G and Fredlund D. G. (2005). “Evolution of the variability of unsaturated properties”. Proceeding of the 58 Canadian Geotechnical conference, Canada. 12(128-135).

Gottardi, G. and Venutelli, M., (1992). “Moving finite element model for one-dimensional infiltration in unsaturated soil”. Water Res. Res., 28(12), pp.3259-3267.

Green, D. K., Douglas, K., & Mostyn, G. (2015). “The simulation and discretisation of random fields for probabilistic finite element analysis of soils using meshes of arbitrary triangular elements”. Comput. Geotech., 68, 91-108.

Gresho, P.M., Lee, R.L., Sani, R.L. and Stullich, T.W., (1978). "Time-dependent FEM solution of the incompressible Navier--Stokes equations in two-and three-dimensions" (No. UCRL-81323; CONF-780712-7). California Univ., Livermore (USA). Lawrence Livermore Lab..

Griffiths, D. V., Fenton, G. A. (1993). "Seepage beneath water retaining structures founded on spatially random soil". Geotechnique, 43(4), 577-87.

Griffiths, D. V., Fenton, G. A. (2007). "The random finite element method (RFEM) in slope stability analysis". Probab. Meth. Geotech. Eng. (pp. 317-346). Springer Vienna.

Griffiths, D. V., Fenton, G. A. (2009). "Probabilistic settlement analysis by stochastic and random finite-element methods". J. Geotech. Geoenv.Eng., 135(11), 1629-1637.

Griffiths, D.V. and Lu, N., (2005). "Unsaturated slope stability analysis with steady infiltration or evaporation using elasto- plastic finite elements". Int. J. Num. Anal. Methods. Geomech, 29(3), pp.249-267.

Guerrero, J.P. and Skaggs, T.H., (2010). "Analytical solution for one-dimensional advection–dispersion transport equation with distance-dependent coefficients". J. Hydrol, 390(1), pp.57-65.

Hills, R.G., Porro, I., Hudson, D.B. and Wierenga, P.J., (1989). "Modeling one-dimensional infiltration into very dry soils: 1. Model development and evaluation". Water Res. Res., 25(6), pp.1259-1269.

Hinton, E., Rock, T. and Zienkiewicz, O.C., (1976). "A note on mass lumping and related processes in the finite element method". Earthquake Eng Struct Dyn, 4(3), pp.245-249.

Hughes TJ. (1978)."The finite element method linear static and dynamic finite element analysis". Dover publ. Inc. Mineola, New York. 445-46.

Hughes, T.J., Cottrell, J.A. and Bazilevs, Y., (2005)." Isogeometric analysis: CAD, finite elements, NURBS, exact geometry and mesh refinement". Comput Methods Appl Mech Eng, 194(39), pp.4135-4195.

Huyakorn, P.S., Springer, E.P., Guvanasen, V. and Wadsworth, T.D., (1986). "A three-dimensional finite- element model for simulating water flow in variably saturated porous media". Water Res. Res., 22(13), pp.1790-1808.

Ilinca, F. and Hétu, J.F., (2008). "A new stabilized finite element method for reaction–diffusion problems: The source- stabilized Petrov–Galerkin method". Int. J. Num. method. Eng, 75(13), pp.1607-1630.

Irzal, F., Remmers, J.J., Verhoosel, C.V. and Borst, R., (2013). "Isogeometric finite element analysis of poroelasticity". Int. J. Numer. Anal. Meth. Geomech., 37(12), pp.1891-1907.

Jaiswal, D.K., Kumar, A. and Yadav, R.R., (2011). "Analytical solution to the one-dimensional advection-diffusion equation with temporally dependent coefficients". J. Water Res. Prot., 3(01), p.76.

Kosugi, K. I. (1996). "Lognormal distribution model for unsaturated soil hydraulic properties". Water Res. Res., 32(9), 2697-2703.

Krabbenhøft, K., (2007). "An alternative to primary variable switching in saturated–unsaturated flow computations". Adv. Water. Res, 30(3), pp.483-492.

Leij, F. J. (1996). "The UNSODA unsaturated soil hydraulic database: user's manual "(Vol. 96, No. 95). National Risk Management Research Laboratory, Office of Research and Development, US Environmental Protection Agency.

Likos, W. J., Lu, N., & Godt, J. W. (2013). "Hysteresis and uncertainty in soil water-retention curve parameters". J. Geotech. Geoenv.Eng., , 140(4), 04013050.

Liu, L. L., Cheng, Y. M., & Zhang, S. H. (2017). "Conditional random field reliability analysis of a cohesion-frictional slope". Comput. Geotech., , 82, 173-186.

Lu, N. and Godt, J.W., (2013). "Hillslope hydrology and stability". Cambridge University Press.

Miller, C.T., Abhishek, C. and Farthing, M.W., (2006). "A spatially and temporally adaptive solution of Richards' equation". Adv. Water Res., 29(4), pp.525-545.

Morgenstern, N. R. (2000). "Performance in geotechnical practice". HKIE Transactions, 7(2), 2-15.

Mualem, Y. (1976). "A new model for predicting the hydraulic conductivity of unsaturated porous media". Water Res. Res, 12(3), 513-522.

Namin, M.M. and Boroomand, M.R., (2012). "A time splitting algorithm for numerical solution of Richard's equation". J. Hydrol, 444, pp.10-21.

Nguyen, M.N., Bui, T.Q., Yu, T. and Hirose, S., 2014. Isogeometric analysis for unsaturated flow problems. Comput. Geotech., 62, pp.257-267.

Oh, W.T. and Vanapalli, S.K., (2012). "Interpretation of the bearing capacity of unsaturated fine-grained soil using the modified effective and the modified total stress approaches". Int. J. Geomech, 13(6), pp.769-778.

Parlange, J.Y., (1971). “THEORY OF WATER-MOVEMENT IN SOILS: 2. ONE-DIMENSIONAL INFILTRATION”. Soil Sc., 111(3), pp.170-174.

Parlange, J.Y., Hogarth, W.L., Barry, D.A., Parlange, M.B., Haverkamp, R., Ross, P.J., Steenhuis, T.S., DiCarlo, D.A. and Katul, G., (1999). “Analytical approximation to the solutions of Richards' equation with applications to infiltration, ponding, and time compression approximation”. Adv. Water Res., 23(2), pp.189-194.

Philip, J.R., (1957). “The theory of infiltration: 4. Sorptivity and algebraic infiltration equations”. Soil sci, 84(3), pp.257-264.

Phoon, K. K. (2004). “Vulnerability and risk associated with geohazards, general non-Gaussian probability models for first-order reliability method (FORM): a state-of-the-art report”. ICG rep no 2004-2-4. International Centre for Geohazards, Oslo, Norway.

Phoon, K. K., & Kulhawy, F. H. (1999). “Characterization of geotechnical variability”. Canad.Geotech. J, 36(4), 612-624.

Phoon, K. K., Santoso, A., & Quek, S. T. (2010). “Probabilistic analysis of soil-water characteristic curves”. J. Geotech. Geoenv. Eng., 136(3), 445-455.

Piegl LA, Tiller W.(1966). “The NURBS Book”. Springer.

Prasad, K.H., Kumar, M.M. and Sekhar, M., (2001). “Modelling flow through unsaturated zones: Sensitivity to unsaturated soil properties”. Sadhana, 26(6), pp.517-528.

Richards, L.A., (1931). “Capillary conduction of liquids through porous mediums”. J. Appl. Phys, 1(5), pp.318-333.

Robinson, J.D. and Vahedifard, F., (2016). “Weakening mechanisms imposed on California’s levees under multiyear extreme drought”. Climatic change, 137(1-2), pp.1-14.

Robinson, J.D., Vahedifard, F. and AghaKouchak, A., (2016). “Rainfall-triggered slope instabilities under a changing climate: comparative study using historical and projected precipitation extremes”. Canad. Geotech. J, 54(1), pp.117-127.

Schweiger, H. F., & Peschl, G. M. (2005). “Reliability analysis in geotechnics with the random set finite element method”. Comput. Geotech., 32(6), 422-435.

Shahraiyni, H.T. and Ashtiani, B.A., (2009). “Comparison of finite difference schemes for water flow in unsaturated soils”. Intl. J. Aerospace and Mech. Eng, 3(1), pp.1-5.

Shahrokhabadi, S., Vahedifard, F. and Ghazanfari, E., (2014). “Modeling flow regime in shale using isogeometric analysis”. In Shale Energy Engineering 2014: Technical Challenges, Environmental Issues, and Public Policy (pp. 239-245).

Sivakumar Babu, G. L., & Murthy, D. S. (2005). “Reliability analysis of unsaturated soil slopes”J. Geotech. Geoenv. Eng., 131(11), 1423-1428.

Soraganvi, V. S., Ababou, R., & Mohan Kumar, M. S. (2016).”Analysis and Upscaling of Unsaturated Flow through Randomly Heterogeneous Soil”. J. Hydr. Eng., 04016063.

Spanos, P.D. and Ghanem, R., (1989). Stochastic finite element expansion for random media. J. Eng. Mech., 115(5), pp.1035-1053.

Srivastava, R. and Yeh, T.C.J., (1991). “Analytical solutions for one- dimensional, transient infiltration toward the water table in homogeneous and layered soils”. Water Res. Res., 27(5), pp.753-762.

Tan, X. H., Hu, N., Li, D., Shen, M. F., & Hou, X. L. (2013). “Time-Variant Reliability Analysis of Unsaturated Soil Slopes Under Rainfall”. Geotech. Geol. Eng., 31(1), 319-327.

Vahedifard, F. and Robinson, J.D., (2015). Unified method for estimating the ultimate bearing capacity of shallow foundations in variably saturated soils under steady flow. J. Geotech. Geoenviron. Eng, 142(4), p.04015095.

Vahedifard, F., Leshchinsky, D., Mortezaei, K. and Lu, N., (2016a). “Effective stress-based limit-equilibrium analysis for homogeneous unsaturated slopes”. Int. J. Geomech, 16(6), p.D4016003.

Vahedifard, F., Mortezaei, K., Leshchinsky, B.A., Leshchinsky, D. and Lu, N., (2016b). Role of suction stress on service state behavior of geosynthetic-reinforced soil structures. Trans. Geotech, 8, pp.45-56.

Valizadeh, N., Bui, T.Q., Vu, V.T., Thai, H.T. and Nguyen, M.N., (2013). “Isogeometric simulation for buckling, free and forced vibration of orthotropic plates”. Int. J. App.l Mech, 5(02), p.1350017.

Van Genuchten, M.T., (1980). “A closed-form equation for predicting the hydraulic conductivity of unsaturated soils”. Soil Sci. Soc. Am. J., 44(5), pp.892-898.

Vo, T., Taiebat, H. and Russell, A.R., (2016). Interaction of a rotating rigid retaining wall with an unsaturated soil in experiments. Géotech, 66(5), pp.366-377.

Warrick, A.W., Islas, A. and Lomen, D.O., (1991). “An analytical solution to Richards' equation for time-varying infiltration”. Water. Resour. Res, 27(5), pp.763-766. 3.

Wu, M. and Gao, L., (1999). “Numerical simulation of saturated–unsaturated transient flow in soils”. J Hyd. Eng, 12, pp.38-42.

Wu, M., (2010). “A finite-element algorithm for modeling variably saturated flows”. J. Hydrol., 394(3), pp.315-323.

Zhang, L., Yan, W. (2015). “Stability Analysis of Unsaturated Soil Slope Considering the Variability of Soil-water Characteristic Curve”. Geotech. Safet . Risk V, 281.

APPENDIX A

CHORD SLOPE APPROXIMATION OF MOISTURE CAPACITY

Chord slope is an alternative and effective approximation of the moisture capacity in contrast of analytical solution. The mass balance error appears in approximating the storage term $\frac{\partial \theta}{\partial t}$ by the expansion $C(\psi)\frac{\partial h}{\partial t}$ in the discretized formulation. If $C(\psi)$ is performed by chord slope approximation instead of analytical derivatives (Eq. (4)), a solution for mass balance error attained. The first-order finite difference approximation for discretized $C(\psi)$ is:

$$C_{t+1}^{\kappa} = \frac{\theta_{t+1}^{\kappa} - \theta_t}{\psi_{t+1}^{\kappa} - \psi_t} \tag{A.1}$$

The limitations for chord slope approximation exist if the denominator of Eq. (2.42) is close to zero. It is recommended to use analytical solution if the denominator is below an absolute minimum difference tolerance (practically, 10^{-18}).

APPENDIX B

SPECIAL MASS LUMPING TECHNIQUE

Hinton et al. (1976) developed the special lumping technique which always generates positive lumped masses by virtue of positive-definiteness. The idea is to set the entries of the lumped-mass matrix proportional to diagonal entries of consistent mass:

$$\boldsymbol{O} = \sum_e \beta \delta_{ij} \int_{\Omega^e} \left(\frac{\theta}{\phi} S_o + C(\psi) \right)^e R_i{}^2 \, d\,\Omega^e \tag{B.1}$$

where

$$\beta = \frac{total\ element\ mass}{\substack{sum\ of\ diagonal \\ entries\ of\ consistent \\ mass}} = \frac{\int_{\Omega^e} \left(\frac{\theta}{\phi} S_o + C(\psi) \right)^e d\Omega^e}{\sum_{i=1}^{n} \int_{\Omega^e} \left(\frac{\theta}{\phi} S_o + C(\psi) \right)^e R_i{}^2 d\Omega^e} \tag{B.2}$$

The special mass lumping has optimal rates of convergence and it is the lumping method that is recommended for arbitrary elements (Hughes, 1978).